Calhoun: The NPS Institutional Archive

DSpace Repository

Theses and Dissertations	1. Thesis and Dissertation Collection, all items

1993-09

An X-ray diffraction investigation of infinity-Al2O3 addition to yttria stabilized zirconia (YSZ) thermal barrier coatings subject to destabilizing vanadium pentoxide (V2O5) exposure

Krestos, Dean M.

Monterey, California. Naval Postgraduate School

https://hdl.handle.net/10945/27339

This publication is a work of the U.S. Government as defined in Title 17, United States Code, Section 101. Copyright protection is not available for this work in the United States.

Downloaded from NPS Archive: Calhoun

http://www.nps.edu/library

Calhoun is the Naval Postgraduate School's public access digital repository for research materials and institutional publications created by the NPS community. Calhoun is named for Professor of Mathematics Guy K. Calhoun, NPS's first appointed -- and published -- scholarly author.

Dudley Knox Library / Naval Postgraduate School
411 Dyer Road / 1 University Circle
Monterey, California USA 93943

DUDLEY KNOX LIBRARY
NAVAL POSTGRADUATE SCHOOL
MONTEREY CA 93943-5101

NAVAL POSTGRADUATE SCHOOL
Monterey, California

THESIS

An X-Ray Diffraction investigation of α-Al_2O_3 addition to yttria stabilized zirconia (YSZ) thermal barrier coatings subject to destabilizing vanadium pentoxide (V_2O_5) exposure

by

Dean M. Krestos

September, 1993

Thesis Advisor: Alan G. Fox

Approved for public release; distribution is unlimited.

REPORT DOCUMENTATION PAGE

Report Security Classification: Unclassified		1b Restrictive Markings			
Security Classification Authority		3 Distribution/Availability of Report Approved for public release; distribution is unlimited.			
Declassification/Downgrading Schedule					
Performing Organization Report Number(s)		5 Monitoring Organization Report Number(s)			
Name of Performing Organization val Postgraduate School	6b Office Symbol *(if applicable)*/N34	7a Name of Monitoring Organization Naval Postgraduate School			
Address *(city, state, and ZIP code)* nterey CA 93943-5000		7b Address *(city, state, and ZIP code)* Monterey CA 93943-5000			
Name of Funding/Sponsoring Organization rderock Division NSWC	6b Office Symbol 34	9 Procurement Instrument Identification Number			
dress *(city, state, and ZIP code)* napolis , MD 21402		10 Source of Funding Numbers			
		Program Element No	Project No	Task No	Work Unit Accession No

Title *(include security classification)*/An X-Ray Diffraction Investigation of α-Al_2O_3 Addition to Yttria Stabilized Zirconia (YSZ) Thermal Barrier Coatings oject to Destabilizing Vanadium Pentoxide (V_2O_5) Exposure.

Personal Author(s) Dean M. Krestos

a Type of Report ster's Thesis	13b Time Covered From To	14 Date of Report *(year, month, day)* September 1993	15 Page Count 80

Supplementary Notation The views expressed in this thesis are those of the author and do not reflect the official policy or position of the Department of fense or the U.S. Government.

Cosati Codes			18 Subject Terms *(continue on reverse if necessary and identify by block number)*
ld	Group	Subgroup	Ceramic, Alpha Alumina, YSZ, Vanadia, Surface-Induced Coating (SIC), PSZ, XRD, SEM

Abstract *(continue on reverse if necessary and identify by block number)*

nce the mid 1970's the U.S. Navy has used Yttria-stabilized zirconia (YSZ) as thermal arrier coatings for hot stage gas turbine components. Use of low cost, high contaminant, uels has led to shortened component life from failure of YSZ coatings due to corrosive ttack by vanadium and other combustion oxides. The object of this investigation was to etermine the reactivity of adding α-Al_2O_3 to current YSZ ceramics for creation of a eramic composite which could improve mechanical properties and show improved durability o corrosive chemical attack. Ten powder samples of $ZrO_2$8mol%Y_2O_3, α-Al_2O_3, and V_2O_5 of arying compositions were annealed at 900°C for 100 hours. X-Ray Diffraction analysis tilizing a standard 'search and match' method was used to determine the phases present in he reacted powder samples. Peak intensity comparisons between reacted and un-reacted amples allowed for a quantitative determination for the reactivity of α-Al_2O_3 with the YSZ ystem exposed to V_2O_5. This investigation indicated that α-Al_2O_3 is non-reactive in all SZ samples exposed to V_2O_5 at 900°C.

Distribution/Availability of Abstract unclassified/unlimited — same as report — DTIC users	21 Abstract Security Classification Unclassified	
a Name of Responsible Individual n G. Fox	22b Telephone *(include Area Code)* (408) 663-3276	22c Office Symbol ME/Fx

) FORM 1473,84 MAR 83 APR edition may be used until exhausted security classification of this page
All other editions are obsolete

Approved for public release; distribution is unlimited.

An X-ray Diffraction investigation of α-Al_2O_3 addition to yttria stabilized zirconia (YSZ) thermal barrier coatings subject to destabilizing vanadium pentoxide (V_2O_5) exposure

by

Dean M. Krestos
Lieutenant, United States Navy
B.S., Miami University, Oxford, OH

Submitted in partial fulfillment
of the requirements for the degree of

MASTER OF SCIENCE IN MECHANICAL ENGINEERING

from the

NAVAL POSTGRADUATE SCHOOL
September 1993

ABSTRACT

Since the mid 1970's the U.S. Navy has used Yttria-stabilized zirconia (YSZ) as thermal barrier coatings for hot stage gas turbine components. Use of low cost, high contaminant, fuels has led to shortened component life from failure of YSZ coatings due to corrosive attack by vanadium and other combustion oxides. The object of this investigation was to determine the reactivity of adding α-Al_2O_3 to current YSZ ceramics for creation of a ceramic composite which could improve mechanical properties and show improved durability to corrosive chemical attack. Ten powder samples of $ZrO_2$8mol%Y_2O_3, α-Al_2O_3, and V_2O_5 were annealed at 900°C for 100 hours. X-Ray Diffraction analysis utilizing a standard 'search and match' method was used to determine the phases present in the reacted powder samples. Peak intensity comparisons between reacted and un-reacted samples allowed for a quantitative determination for the reactivity of α-Al_2O_3 with the YSZ system exposed to V_2O_5. This investigation indicated that α-Al_2O_3 is non-reactive in all YSZ samples exposed to V_2O_5 at 900°C.

AF862418

TABLE OF CONTENTS

I. **INTRODUCTION** 1

II. **BACKGROUND** 2

A. CRYSTALLOGRAPHY OF ZIRCONIA 2

1. Cubic 2

2. Tetragonal 4

3. Monoclinic 4

B. CRYSTALLOGRAPHY OF ALUMINA 5

C. MECHANICAL PROPERTIES OF ZIRCONIA SYSTEMS . . . 6

D. BINARY PHASE DIAGRAMS OF ZrO_2-Al_2O_3-Y_2O_3-V_2O_5 SYSTEMS 7

1. ZrO_2-Y_2O_3 Phase Diagram 7

a. Monoclinic → Tetragonal Transformation 9

b. Cubic → Tetragonal Transformation . . 10

2. ZrO_2-V_2O_5 Phase Diagram 10

3. Al_2O_3-ZrO_2 Phase System 11

4. Al_2O_3-Y_2O_3 Phase Diagram 11

5. Al_2O_3-V_2O_5 Phase Diagram 12

6. Y_2O_3-V_2O_5 Phase Diagram 13

7. Additional Stabilizing Oxides for Zirconia 14

E. DESTABILIZATION OF YSZ BY CHEMICAL ATTACK . . . 16

DUDLEY KNOX LIBRARY
NAVAL POSTGRADUATE SCHOOL
MONTEREY CA 93943-5101

1. Reaction of Vanadium Compounds With Ceramic Oxides 16

2. Reaction of V_2O_5 With ZrO_2 17

3. Reaction of V_2O_5 With Y_2O_3 17

4. Reactions of YSZ With Vanadium Pentoxide . 18

III. FABRICATION PROCESS FOR THERMAL BARRIER COATINGS 21

A. PLASMA SPRAY COATING 21

B. SURFACE INDUCED COATING METHOD 25

IV. SCOPE OF PRESENT WORK 30

V. EXPERIMENTAL PROCEDURE 31

A. SAMPLE PREPARATION 31

B. X-RAY DIFFRACTION 31

C. SCANNING ELECTRON MICROSCOPY (SEM) 33

VI. RESULTS AND DISCUSSION 35

A. X-RAY DIFFRACTION RESULTS 35

1. YSZ-Al_2O_3-V_2O_5 Unreacted Powder Samples . . 35

2. YSZ-Al_2O_3-V_2O_5 Annealed Powder Samples . . 35

a. Destabilization of ZrO_2 36

b. Ytria Vanadate (YVO_4) Formation 45

c. V_2O_5 Intensity 45

d. α-Al_2O_3 Intensity 45

B. SEM RESULTS 54

VII. CONCLUSIONS 61

VIII. RECOMMENDATIONS 62

LIST OF REFERENCES 64

INITIAL DISTRIBUTION LIST 67

LIST OF TABLES

TABLE I. ROOM TEMPERATURE TOUGHNESS K_{Ic} AND STRENGTH σ_f OF ZrO_2 TOUGHENED CERAMICS 6

TABLE II. POWDER SAMPLES OF THE $ZrO_2$8mol.%Y_2O_3-Al_2O_3-V_2O_5 SYSTEM BY WEIGHT PERCENT 34

TABLE III. ANNEALED POWDER SAMPLES OF THE $ZrO_2$8mol.%Y_2O_3-Al_2O_3-V_2O_5 SYSTEM BY ATOMIC PERCENT 38

TABLE IV. PEAK INTENSITY VALUES FOR (111) MONOCLINIC ZrO_2 BY INCREASING ATOMIC PERCENT ZrO_2 42

TABLE V. PEAK INTENSITY VALUES FOR (200) TETRAGONAL YVO_4 BY INCREASING ATOMIC PERCENT YVO_4 48

TABLE VI. PEAK INTENSITY VALUES FOR (113) α-Al_2O_3 UNREACTED AND REACTED SAMPLES BY INCREASING ATOMIC PERCENT α-Al_2O_3 52

LIST OF FIGURES

Figure 1. System ZrO_2 3

Figure 2. Schematic diagrams of fluorite structure of cubic zirconia 3

Figure 3. Crystal structure of monoclinic and tetragonal ZrO_2 4

Figure 4. Hexagonal closed-packed structure of α-alumina 5

Figure 5. System ZrO_2-Y_2O_3 8

Figure 6. Low Yttria region of ZrO_2-Y_2O_3 system 8

Figure 7. System V_2O_5-ZrO_2 10

Figure 8. System Al_2O_3-ZrO_2 11

Figure 9. System Al_2O_3-Y_2O_3 12

Figure 10. System V_2O_5-Al_2O_3 12

Figure 11. System Y_2O_3-V_2O_5 13

Figure 12. System ZrO_2-MgO 14

Figure 13. Zirconia - calcia binary system 15

Figure 14. System ZrO_2-Sc_2O_3 15

Figure 15. Reaction behavior and products of ceramic oxides with vanadium pentoxide 17

Figure 16. Concentration variations for yttrium, vanadium, and zirconium on single crystal samples . . . 20

Figure 17. Schematic of low-pressure plasma deposition (LPPD) method 22

Figure 18. Cross-section of plasma-sprayed Thermal barrier coating test sample 23

Figure 19. Schematic representation of Surface Induced Coating (SIC) method 26

Figure 20. SEM micrographs of Zirconia Toughened Alumina (ZTA) samples prepared by SIC and conventional methods 27

Figure 21. Grain size distribution of Al_2O_3 and ZrO_2 in ZTA samples processed by SIC and conventional fabrication methods 29

Figure 22. Plot of sample number four (60%YSZ-30%Al_2O_3-10%V_2O_5) and corresponding diffraction patterns for SCHERBINAITE, CORUNDUM, and tetragonal ZrO_2 . 37

Figure 23. Comparison of sample number one (80%YSZ-10%Al_2O_3-10%V_2O_5) unreacted and reacted samples showing the three polymorph diffraction patterns for ZrO_2 39

Figure 24. Measurement for percent destabilization for sample number one 40

Figure 25. Peak intensity for monoclinic ZrO_2 (111) versus atomic percent monoclinic ZrO_2 43

Figure 26. Plot of unreacted and reacted sample number two showing both monoclinic and tetragonal ZrO_2 peaks 44

Figure 27. Plot of unreacted and reacted sample number one showing YVO_4 formation and peak intensity line for YVO_4 at the (200) reflection plane 47

Figure 28. Plot of peak intensity of YVO_4 versus atomic percent YVO_4 49

Figure 29. Plot of sample number eight V_2O_5 peak intensity (001) reflecting plan 50

Figure 30. Comparison of unreacted and reacted sample number three peak intensity values for (113) α-Al_2O_3 reflecting plane 51

Figure 31. Plot of peak intensity (113) α-Al_2O_3 for unreacted and reacted samples versus atomic percent α-Al_2O_3 53

Figure 32. SEM photograph of wide field view of sample number ten (X528) 55

Figure 33. SEM photograph of closeup view of ZrO_2 agglomerate from sample number ten (X 1,32K) 56

Figure 34. SEM photograph of matrix surface of sample number ten (X1,35K) 57

Figure 35. SEM photograph of crystalline structure of sample number ten (X462) 59

Figure 36. SEM photograph of amorphous glassy phase of sample number ten (X236) 60

ACKNOWLEDGEMENTS

I would like to express my sincere appreciation to my advisor Professor Alan G. Fox for his guidance and assistance in helping me to complete this thesis.

I would like to dedicate this thesis to all my loved ones who have supported me during my time of study while at the Naval Postgraduate School. Specifically my parents, godparents, and children, Alexis, Andrea, and Michael who understood the need for their father to spend so many nights and weekends away from them studying at school. Last, my beautiful wife Estelle, whose love and encouragement were instrumental for me in my completion of this study; who along with Peter could have made things easier on me by giving me all the answers, but allowed me to work it out for myself and truly learn a thing or two!

I. INTRODUCTION

Since the mid 1970's the U.S. Navy has been utilizing thermal barrier coatings (TBC) on hot stage gas turbine superalloy components. Yttria stabilized zirconia (YSZ) has been effective in providing thermal barrier protection, allowing for realized increases in operating temperatures from 50-220°C, thereby obtaining increases in engine efficiencies from 10 to 15 percent [Ref. 1]. Many researchers have found that YSZ becomes highly unstable and prematurely fails when exposed to inorganic fuel contaminants such as vanadium and sulphur which are found in low cost fuels of non-aviation quality. Vanadium can be found in fuels in the form of vanadium porphyrin which is transformed during combustion into $VO(OH)_3$ (gas) and V_2O_5 (solid) [Ref. 2]. Vanadium pentoxide (V_2O_5) is in liquid form at 672°C and reacts with the stabilizing agent Y_2O_3 to form yttria vanadate (YVO_4). This reaction leaves behind an unstable tetragonal (t) zirconia structure which transforms to monoclinic (m) zirconia while cooling to room temperature. The $t \rightarrow m$ transformation results in a 4-5 percent volume increase within the matrix leading to spalling and eventual premature failure of the coating [Ref. 3]. The emphasis of the current research is to investigate alpha alumina (α-Al_2O_3) as a possible additive to the current YSZ ceramic for the creation of a composite which could show improved immunity to corrosive attack and improved durability to thermal cycling.

II. BACKGROUND

In order to interpret data on composites containing ZrO_2, V_2O_5, Al_2O_3, and Y_2O_3, it is necessary to understand all the binary and ternary phase diagrams of these systems and the crystallography of the phases present. The first section of this background will therefore be devoted to summarizing these fundamentals.

A. CRYSTALLOGRAPHY OF ZIRCONIA

Pure zirconia exhibits three different crystal structures at atmospheric pressure as shown in Figure 1 [Ref. 4].

1. Cubic

The cubic phase is the first polymorph to form from the liquidus state at 2680 $\pm$ 15°C. Cubic zirconia has the fluorite crystal structure which is FCC. Eight anions (oxygen) are located equidistantly at the eight tetrahedral positions. Each anion is tetrahedrally surrounded by four cations (zirconia) as seen in Figure 2 [Ref. 1]. Cubic zirconia is stable down to 2370°C.

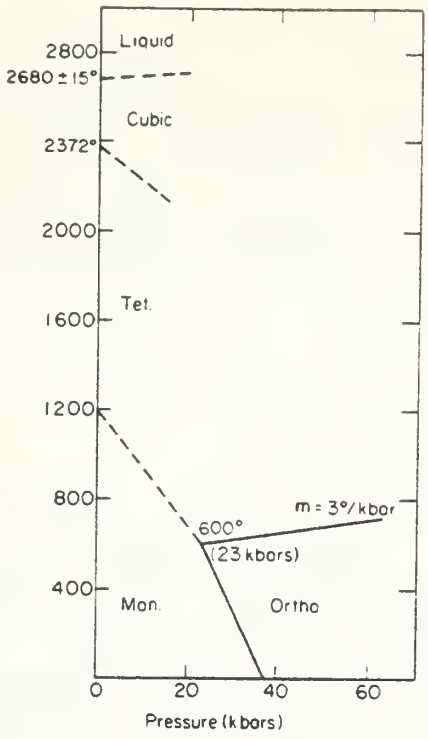

Figure 1. System ZrO_2.

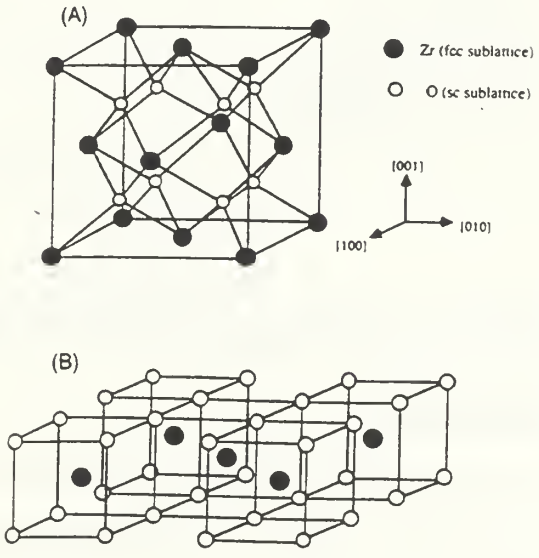

Figure 2. Schematic diagrams of fluorite structure of cubic ZrO_2 emphasizing (A) face-centered cubic packing of cation sublattice and (B) simple cubic packing of anion sublattice.

2. Tetragonal

The tetragonal (t) polymorph forms at 2370°C and is stable through 1170°C. The cation is surrounded by eight anions, four equidistantly at 0.2465 nm and the other four at 0.2065 nm. This structure is classified as simple tetragonal and is shown in Figure 3 [Ref. 5:p. 96].

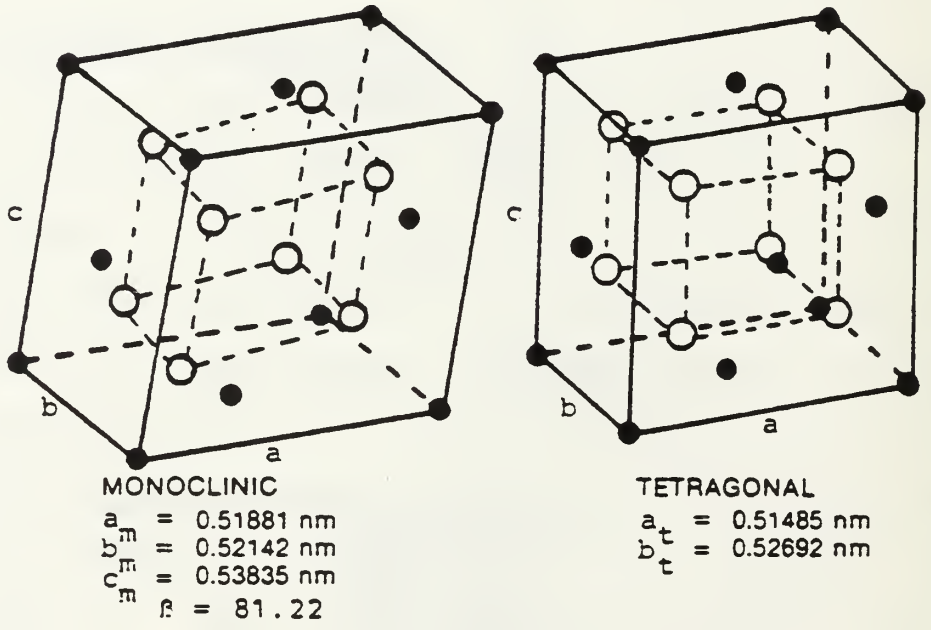

Figure 3. Crystal structures of monoclinic and tetragonal zirconia with lattice parameters at 950°C for both phases.

3. Monoclinic

The monoclinic phase is stable at all temperatures below 1170°C. The cation has a coordination number of seven which indicates a departure from pure ionic bonding, suggesting that covalent bonding is present [Ref. 6]. The simple monoclinic

bravais lattice is shown in Figure 3.

B. CRYSTALLOGRAPHY OF ALUMINA

Alpha alumina (tradename corundum) is an excellent candidate for addition to the YSZ system due to it's properties of high elastic moduli, low density, and most importantly it's stability at extremely high temperatures [Ref. 7]. Corundum has the hexagonal close packed structure as shown in Figure 4 [Ref. 7].

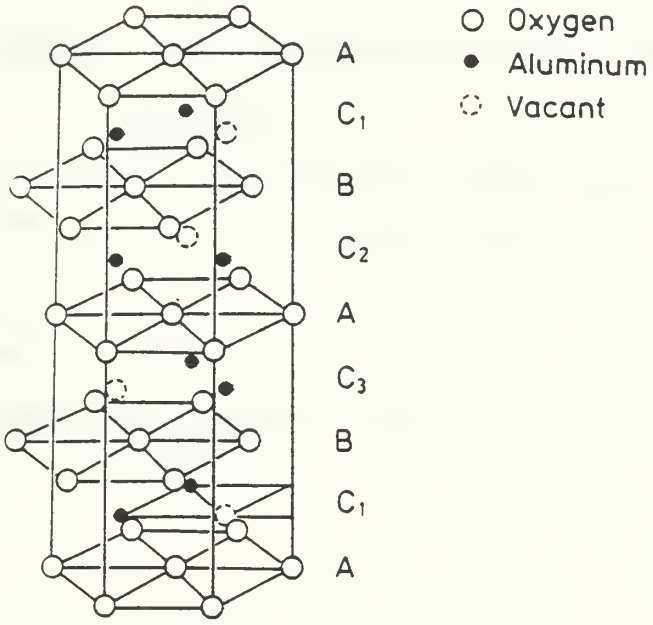

Figure 4. Hexagonal closed-packed structure of α-alumina. A & B layers contain oxygen atoms. C_1, C_2, and C_3 contain aluminum atoms. The C layers are only two-thirds full.

C. MECHANICAL PROPERTIES OF ZIRCONIA SYSTEMS

As a ceramic, zirconia presents an attractive package of properties; high strength at extremely high temperatures, low density, and chemical inertness due to its ionic nature. The achilles heel for this and other ceramics is the absence of toughness. Ceramics are prone to catastrophic failures from minute internal or external flaws. TABLE I presents very promising possibilities for the creation of ceramic matrix composites (CMC) [Ref. 8 pg. 24].

TABLE I.

ROOM TEMPERATURE TOUGHNESS K_{Ic} AND STRENGTH σ_f OF ZrO_2-TOUGHENED CERAMICS

Ceramic Material	Matrix alone		Matrix + ZrO_2	
	K_{Ic} (MPa $m^{1/2}$)	σ_f (MPa)	K_{Ic} (MPa $m^{1/2}$)	σ_f (MPa)
c-ZrO_2	2.4	180	2 - 3	200-300
PSZ			6 - 8	600-800
TZP			7 - 12	1000-2500
Al_2O_3	4	500	5 - 8	500-1300

PSZ - Yttria Stabilized Zirconia

TZP - Tetragonal Stabilized Zirconia

The effect of 'alloying' ceramic particles or fibers are clearly evident. The fracture toughness values show an increase of nearly 300 percent, likewise rupture strengths have been shown to produce similar increases for ZrO_2 toughened ceramics. Contributions to the increased toughness and strength values are from different mechanisms, e.g., the stress-induced t → m transformation (process zone mechanism), microcracking, crack deflection and bridging (from whisker composites), and inhibition of grain growth (grain boundary pinning).

D. BINARY PHASE DIAGRAMS OF ZrO_2-Al_2O_3-Y_2O_3-V_2O_5 SYSTEMS

The use of binary phase diagrams is sufficient as a starting point when evaluating multiple compound formations. Unfortunately, the availability of ternary phase diagrams for the ZrO_2-Al_2O_3-Y_2O_3 system was extremely limited. One was obtained, but for a temperature of 1450°C [Ref. 9], well above the temperature of interest for this research.

1. ZrO_2-Y_2O_3 Phase Diagram

The zirconia-yttria system is one of the most well known systems due to the extensive research in the field of thermal barrier coatings. Figure 5 shows clearly that with an increasing amount of Y_2O_3 the cubic solid solution phase greatly expands, producing a stable cubic phase to about 300°C (at 25mol%Y_2O_3) [Ref. 10]. A clearer view of the low-yttria region is depicted in Figure 6 [Ref. 11]. Yttria content below 4-5 percent creates the monoclinic polymorph upon cooling. Yttria percentages above 15

percent produce a fully stabilized zirconia (FSZ) at room temperatures.

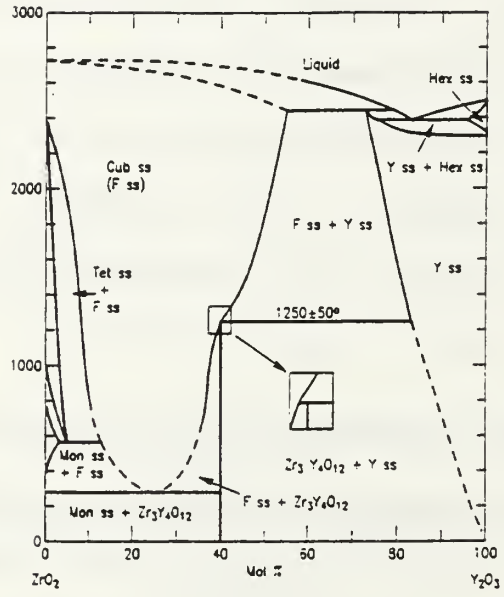

Figure 5. System ZrO_2-Y_2O_3. F = fluorite type of ZrO_2; Y = Y_2O_3; Cub = cubic; Tet = tetragonal; Mon = monoclinic; Hex = hexagonal.

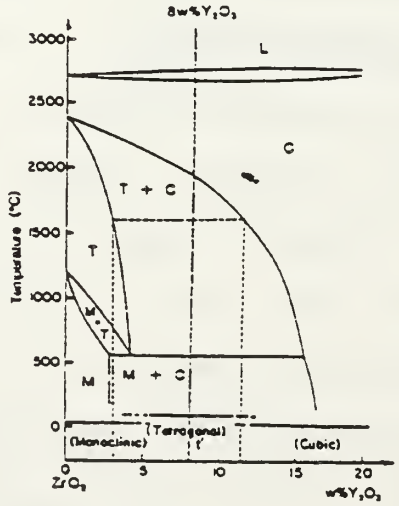

Figure 6. Low yttria region of the zirconia-yttria phase diagram.

FSZ are produced for their stability and strength at room temperature and widely used in costume jewelry as diamond replacements. The phase desired near room temperature has a yttria content of between 6-12 mole percent. The tetragonal phase is desired because it is metastable and does not spontaneously transform into monoclinic upon cooling.

The monoclinic structure is not desired due to the 4-5 percent volume increase during cooling, this would create undue stresses in the matrix and cause coating failure. The FSZ structure is undesirable because it does not have the microstructural defects, specifically twinning of the tetragonal grains and production of anti-phase boundaries (APB), or show coherent precipitates at high annealing temperatures like the tetragonal phase. [Ref. 11] These microstructural defects of tetragonal zirconia allow for the dissipation of crack propagation energy through a crack deviation mechanism not found in the other two polymorphs. These phenomena explain why researchers have settled on eight (8) mole percent yttria as the optimum content for zirconia stabilization.

a. Monoclinic → Tetragonal Transformation

This transformation was determined by high temperature X-Ray Diffraction in 1929. Wolten was the first to suggest that this was a diffusionless 'martensitic like' transformation. A hysterisis effect exists with a forward transition temperature of 950°C and a reverse transformation temperature of 1170°C. This martensitic transformation can occur athermally or by stress-inducement (as found in the region of a

stress field ahead of a crack tip). [Ref. 12]

b. Cubic → Tetragonal Transformation

This displacive transformation is composition invariant and occurs with a change in crystal structure relative to the parent cubic phase (resulting in a strain free, undisturbed habit plane) [Ref. 11] and [Ref. 12]. Other characteristics of this transformation are a homogenous shape change due to the shear action which is reflected by surface relief where the product regions form. Twinning also occurs with this transformation in polycrystalline materials.

2. ZrO_2-V_2O_5 Phase Diagram

The ZrO_2-V_2O_5 system shown in Figure 7 indicates low liquidus temperatures for high concentrations of V_2O_5 with a eutectic and peritectic based on pure ZrO_2 and ZrV_2O_7 [Ref. 13]. The stoichiometric structure ZrV_2O_7 (zirconium vanadate - cubic structure) will be shown later to develop over extended periods of time and is therefore unlikely to be as detrimental to a YSZ coating as the formation of YVO_4.

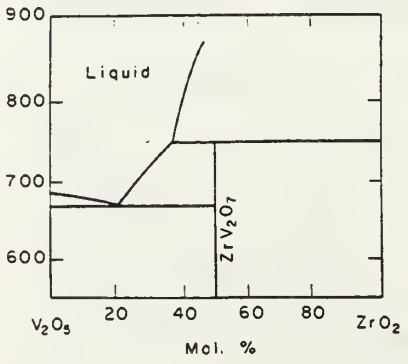

Figure 7. System V_2O_5-ZrO_2.

3. Al_2O_3-ZrO_2 Phase System

One of the most promising aspects of corundum as an additive for ceramic matrix composites is its high temperature stability as indicated in Figure 8 [Ref. 14]. The eutectic point for the Al_2O_3-ZrO_2 system is nearly 1000°C above the typical gas turbine operating temperature. Whether as a polycrystalline powder or fabricated whisker, α-alumina and zirconia remain in solidus form up to 1845°C, and appear to be immiscible in the solid state.

4. Al_2O_3-Y_2O_3 Phase Diagram

The Al_2O_3-Y_2O_3 phase diagram indicates that the various phases which can form are all solid at temperatures of interest in the present work as seen in Figure 9 [Ref. 15]. Of interest are the garnet structure (3:5 ratio) and the perovskite structure (1:1 ratio). Perovskite is a complex structure which is found in several electrical ceramics.

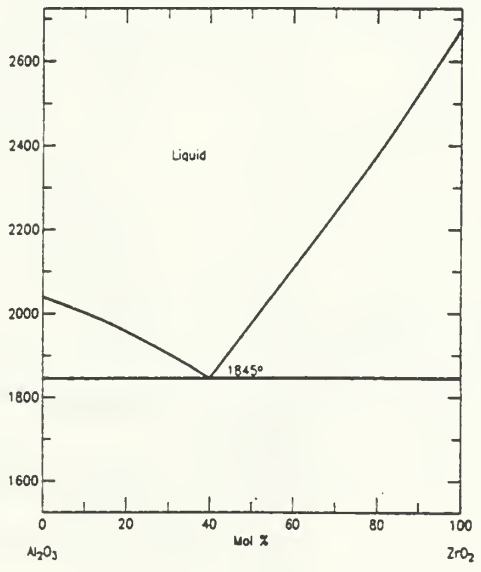

Figure 8. System Al_2O_3-ZrO_2 Phase Diagram.

5. Al_2O_3-V_2O_5 Phase Diagram

The Al_2O_3-V_2O_5 system shown in Figure 10 exhibits no propensity for stoichiometric compound formation, and remains in the solidus phase below the 660°C eutectic temperature. [Ref. 17]

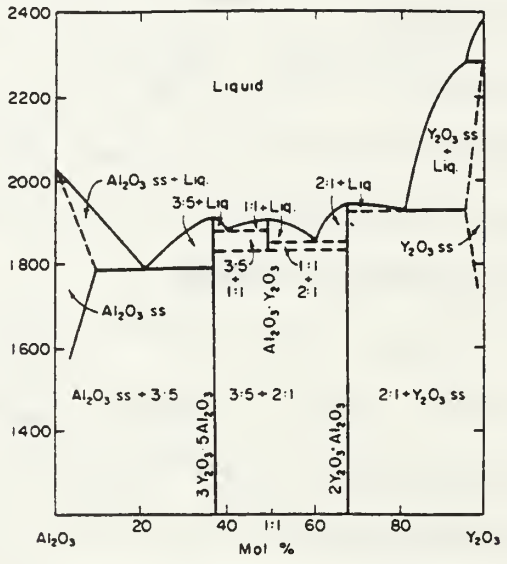

Figure 9. System Al_2O_3-Y_2O_3, tentative. $3Y_2O_3*5Al_2O_3$ (3:5) = garnet structure type; $Y_2O_3*Al_2O_3$ (1:1) = perovskite; $2Y_2O_3*Al_2O_3$ (2:1) = monoclinic symmetry.

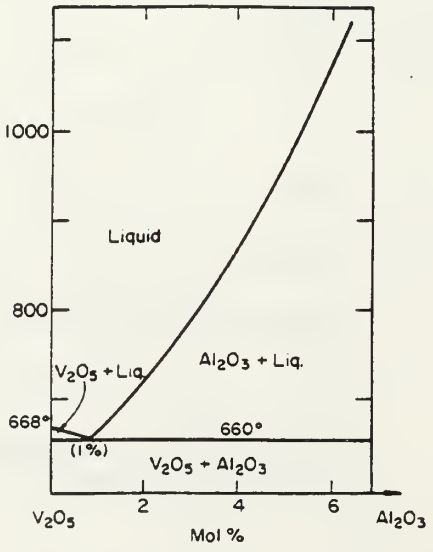

Figure 10. System V_2O_5-Al_2O_3.

6. Y_2O_3-V_2O_5 Phase Diagram

The Y_2O_3-V_2O_5 phase diagram is one of the most important diagrams in helping to explain the deleterious effects of vanadium pentoxide on yttria stabilized zirconia. The formation of yttria vanadate (YVO_4) is possible for all percentages of V_2O_5 above 20 percent for operating temperatures of interest. Since V_2O_5 is a combustion byproduct it is obvious that cheaper fuels (less processing) will contain higher amounts of vanadium porphyrin. The Y_2O_3-V_2O_5 phase diagram is shown in Figure 11 [Ref. 18].

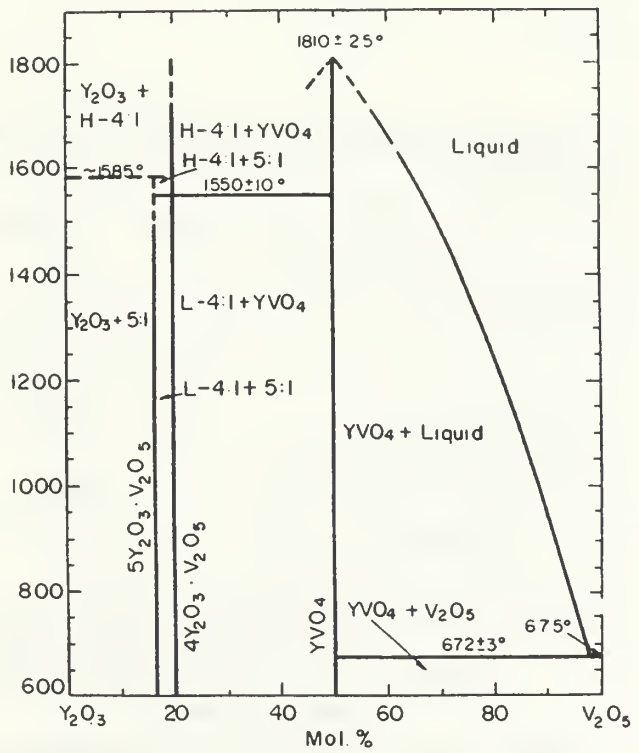

Figure 11. System Y_2O_3-V_2O_5. The Y_2O_3-YVO_4 subsystem is probably pseudobinary because of oxygen losses from the 4:1 and 5:1 phases. L and H = low and high forms respectively.

7. Additional Stabilizing Oxides for Zirconia

Oxides of calcia, magnesia, india, and scandia have also been seen to demonstrate a stabilizing effect on zirconia because of their high solubility in zirconia and ability to form the fluorite type structure. Current research with india (I_2O_3) and scandia (Sc_2O_3) have shown improvements over yttria from the destabilizattion of zirconia due to YVO_4 production and associated leaching of the zirconia matrix [Ref. 19]. Three of these common zirconia stabilizers, MgO, CaO, and Sc_2O_3 are shown below in Figure 12 [Ref. 20], Figure 13 [Ref. 10], and Figure 14 [Ref. 21], respectively.

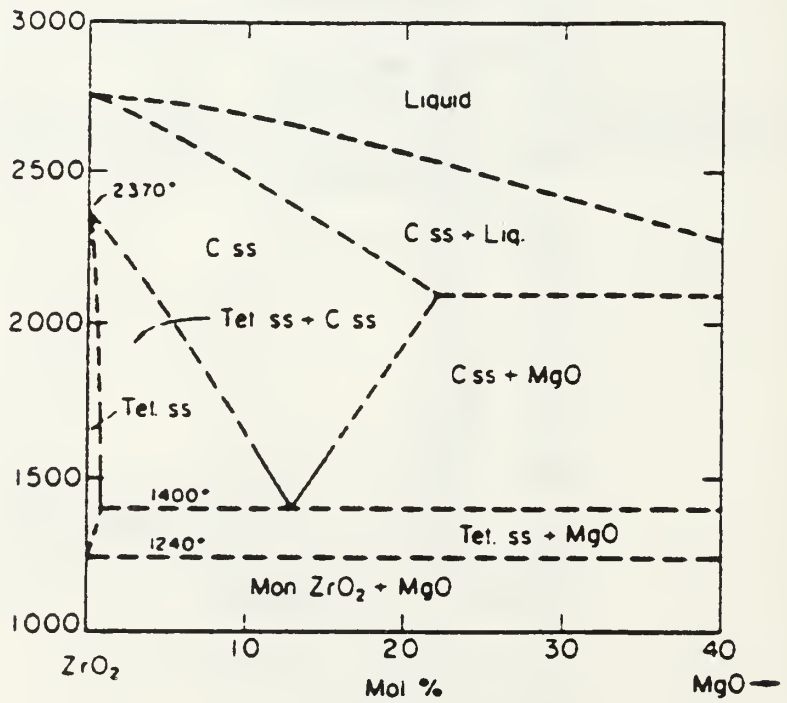

Figure 12. System ZrO_2-MgO showing ZrO_2-rich side.

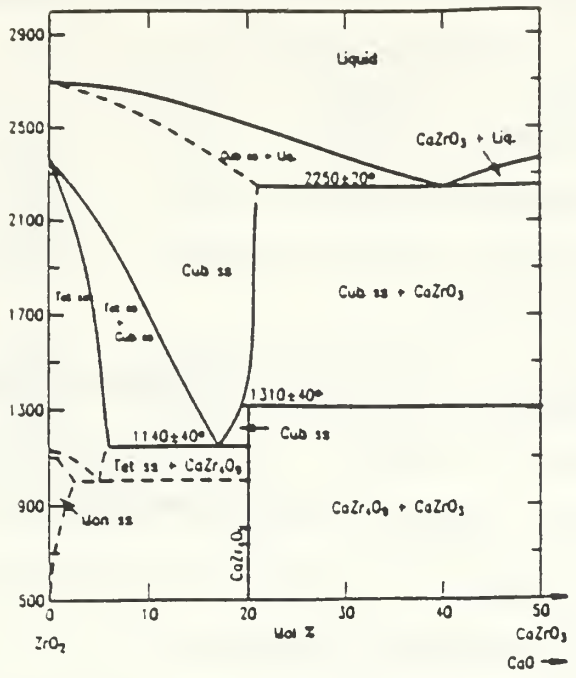

Figure 13. Zirconia-calcia binary system.

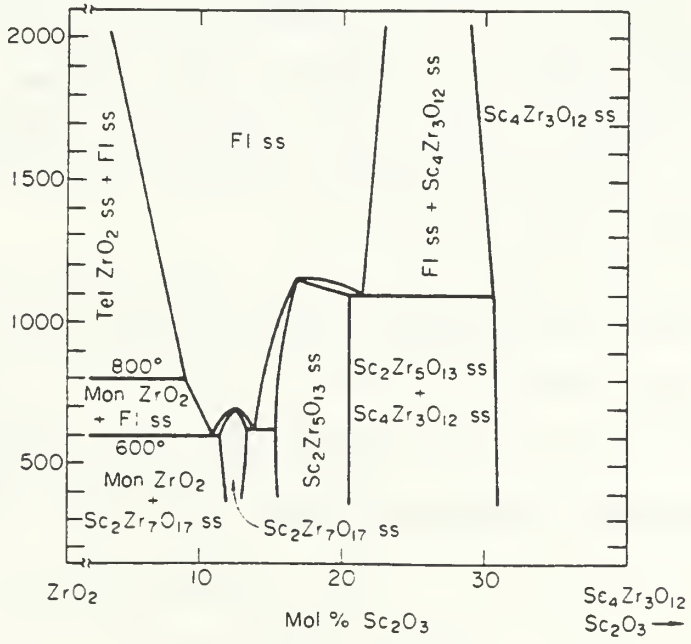

Figure 14. System ZrO_2-Sc_2O_3, partial subsolidus. *Fl ss* = flourite-type cubic ss: *Mon* = monoclinic; *Tet* = tetragonal. $Sc_2Zr_7O_{17}$, $Sc_2Zr_5O_{13}$, and $Sc_4Zr_3O_{12}$ show rhombohedral symmetry.

E. DESTABILIZATION OF YSZ BY CHEMICAL ATTACK

Fuel contaminants that are known to cause corrosive attack on ceramics are vanadium, sulphur, sodium, and phosphorous. All of these contaminants form oxide species during combustion (V_2O_5, SO_3, Na_2O, and P_2O_5) [Ref. 22]. Of specific interest to this research is V_2O_5.

1. Reaction of Vanadium Compounds With Ceramic Oxides

Ceramic oxides have particular acid or base characteristics. Lewis acid-base theory is used to explain the tendency for oxides to react with each other. R. L. Jones describes Lewis acid-base theory as:

> Basicity is defined as the ability to donate electronic charge and acidity as the ability to accept electronic charge. For oxides, the oxide anion is the charge donor, and it's behavior is modified by the cation, where the cation acidity increases both as the cation positive charge increases and the cationic radii decreases.... Thus, each oxide species has a characteristic acidity (or basicity), and the tendency for reaction between oxides will depend, to a first approximation, on the difference between their relative acid or base strengths. [Ref. 22 pg. 371]

Reactions of some vanadium compounds with ceramic oxides and their products are shown in Figure 15 [Ref. 22]. This figure clearly indicates the notion that based on Lewis acid-based theory, acids will react with bases, but not acids with acids nor bases with bases.

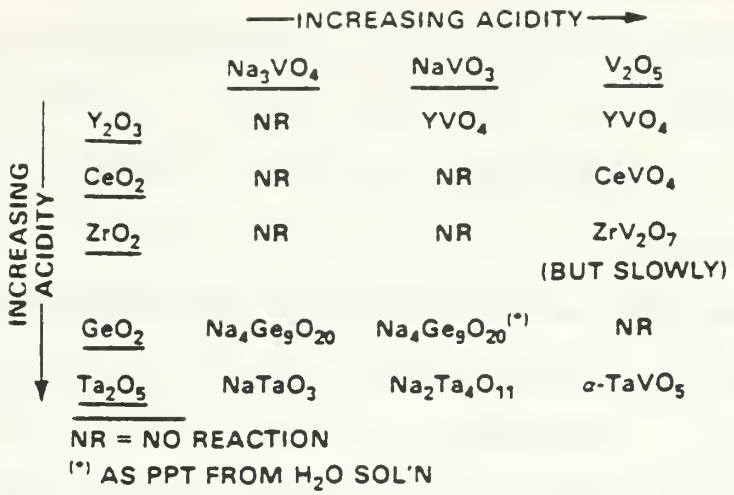

Figure 15. Reaction behavior and products of ceramic oxides with vanadium compounds.

2. Reaction of V_2O_5 With ZrO_2

Based on the phase diagram in Figure 7, the proposed reaction for the V_2O_5-ZrO_2 system would be:

$$V_2O_5 + ZrO_2 = ZrV_2O_7 \quad (1)$$

As shown by Figure 15, ZrV_2O_7 forms but only after a long period of time and/or high temperature ZrO_2 exposure to vanadium pentoxide.

3. Reaction of V_2O_5 With Y_2O_3

Assuming that V_2O_5 and Y_2O_3 react on an equimolar basis, the creation of yttria vanadate is:

$$V_2O_5 + Y_2O_3 = 2YVO_4 \quad (2)$$

As shown in the phase diagram (Figure 10), YVO_4 can form with V_2O_5 concentrations above 20 percent. It is not surprising

that from Lewis acid-base theory that YVO_4 rapidly forms as Y_2O_3 is very basic relative to V_2O_5 acidity. This important principle is a major reason why researchers are viewing alternative stabilizers such as scandia (Sc_2O_3) and india (I_2O_3) as alternative zirconia stabilizers. Both of these oxides, on a relative basis, are more acidic than yttria.

4. Reactions of YSZ With Vanadium Pentoxide

The reaction between V_2O_5 and Y_2O_3 occurs within the zirconia matrix. Rewriting equation (2):

$$Y_2O_3 \text{ (base)} + V_2O_5 \text{ (acid)} = 2YVO_4 \text{ (salt)} \quad (3)$$

$$Y_2O_3 \text{ (a<1)} + V_2O_5 \text{ (a<1)} = 2YVO_4 \text{ (s,a=1)} \quad (4)$$

$$Y_2O_3 \text{ } (ZrO_2) + V_2O_5 \text{ (melt)} = 2YVO_4 \text{ (ppt.)} \quad (5)$$

Equation (3) is written to emphasize the Lewis acid-base nature specific to corrosive chemical attack on ceramics. [Ref. 23]. Equation (4) emphasizes that the activities of yttrium oxide in PSZ and vanadium pentoxide in melt are less than one (a<1), and the yttria vanadate is formed as a pure solid with activity equal to one (s, a=1) [Ref. 23].

Equation (5) indicates the physical nature of the corrosive attack. Molten V_2O_5 attaches to the YSZ surface. The zirconia matrix (as well as other oxide ceramics) surface is porous, allowing the molten salt to thoroughly penetrate the matrix surface [Ref. 23].

Diffusion of vanadium into the matrix (near the surface) precipitates the YVO_4 formation on the surface, creating a depletion zone within the interior of the surface. Depletion of

Y_2O_3 from the zirconia matrix creates the unstable condition for the low temperature transformation of the desirable polymorph of ZrO_2 (tetragonal and cubic) to monoclinic ZrO_2 on the surface. Cracks initiate due to the cubic → tetragonal → monoclinic transformations associated with the thermal cycling from continued transformations. This repeated cycling will allow the cracks to grow and branch into the coating interior eventually leading to spalling and final coating failure. [Ref. 22]

Work by Patton et al on single crystal yttria stabilized zirconia exposed to vanadium pentoxide melts are presented in Figure 16 and illustrates this behavior [Ref. 22].

(a)

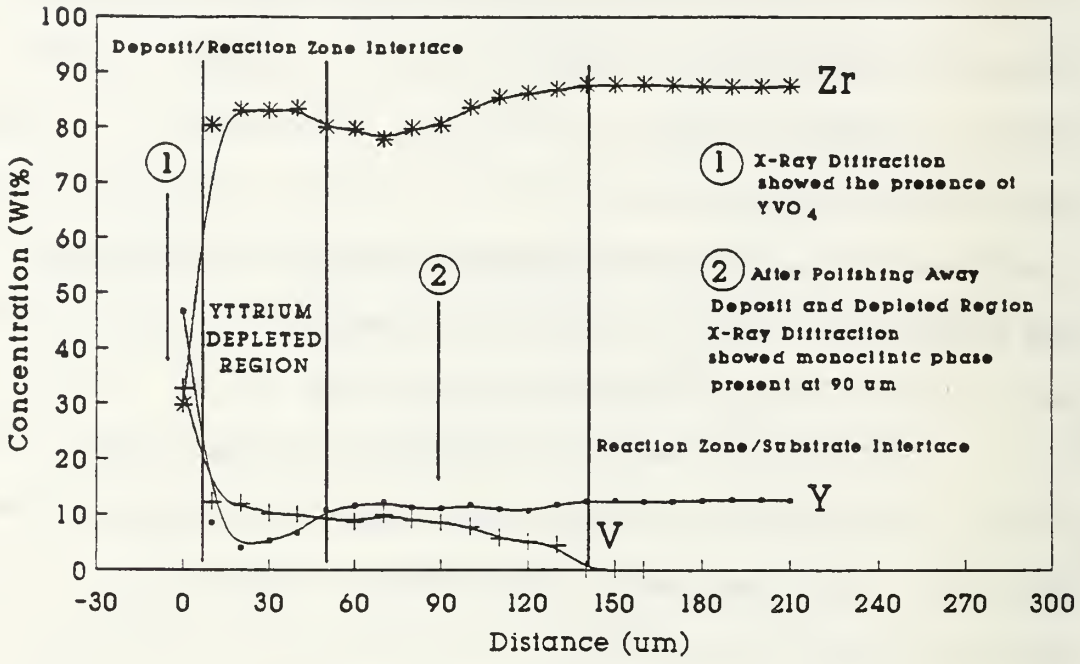

(b)

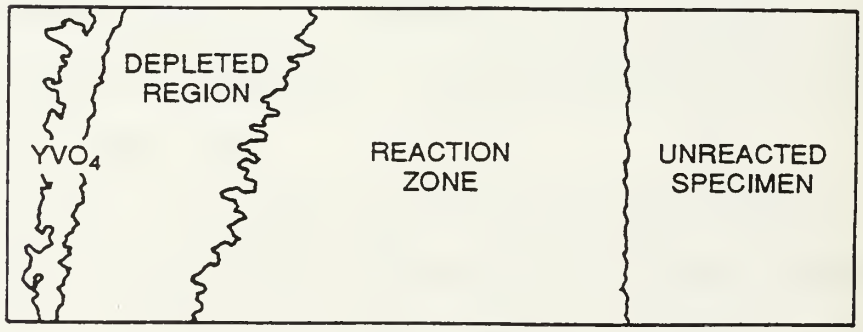

Figure 16. A comparison of (a) the concentration variations for yttrium, vanadium and zirconium existing in a YSZ specimen afterexposure to V_2O_5 for 100 hours using EPMA compared to (b) a schematic illustrating the orientation of the different regions.

III. FABRICATION PROCESS FOR THERMAL BARRIER COATINGS

One important feature of any potential coating is its method of application. Current researchers have recently looked at the fabrication process of TBCs as a way of improving the durability and mechanical properties of these coatings. Recent work with Al_2O_3-ZrO_2-$SiC_{(w)}$ whisker composites utilizing the Surface Induced Coating (SIC) method have shown promising results in mechanical properties strengthening [Ref. 24]. The increased strength arises from the fabrication of a uniform spatial distribution of ZrO_2 and $SiC_{(w)}$ phases throughout the Al_2O_3 matrix. This homogenous fabrication method also shows the promise of minimizing the t → m zirconia transformation due to the suppression of tetragonal grain growth within the matrix not enabling the tetragonal grain to reach the critical grain diameter (d_c) [Ref. 8], [Ref. 24], and [Ref. 25]. Colloidal processing techniques should be another aspect to consider with the addition of α-Al_2O_3 to the $ZrO_2$8mol%Y_2O_3 matrix.

A. PLASMA SPRAY COATING

The plasma spray deposition method is widely used in the fabrication/application of thermal barrier coatings [Ref. 26]. Plasma spray deposition can evenly distribute ultra thin coatings of material and join dissimilar materials which are difficult to bond. A low-pressure plasma deposition (LPPD) system is depicted in Figure 17 [Ref. 7].

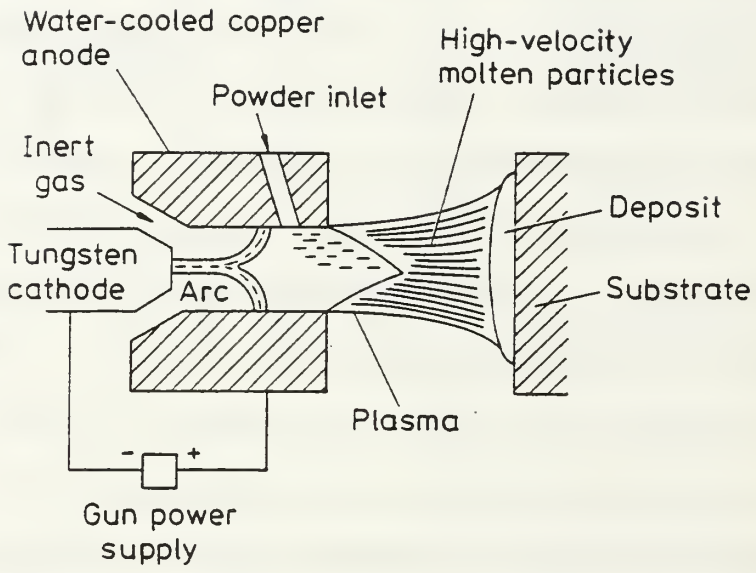

Figure 17. Schematic of low-pressure plasma deposition (LPPD) method.

Due to the large difference in the coefficients of thermal expansions (C.T.E.) between ceramic oxides and metallic superalloys, an intermediate bondcoat is necessary to minimize the surface/interface shear strains due to expansion and contraction of the interface due to thermal cycling. Figure 18 shows a typical cross-section of a partially stabilized zirconia thermal barrier coating on a superalloy substrate [Ref. 23].

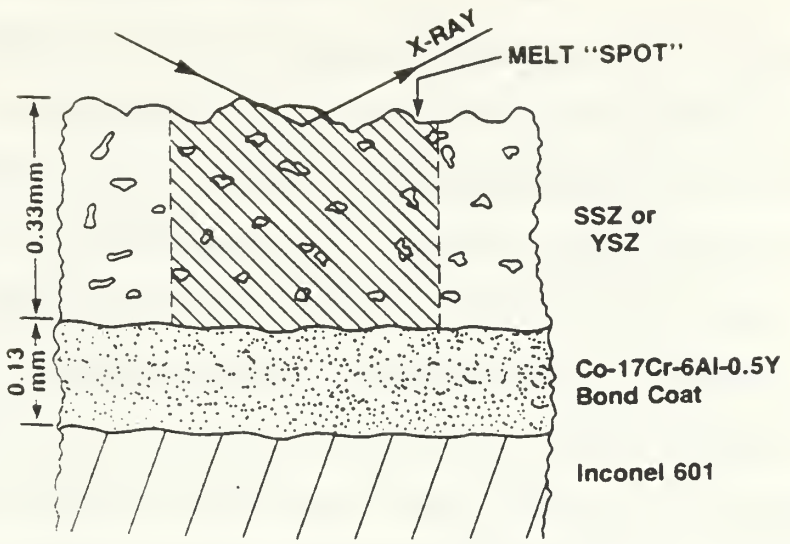

Figure 18. Cross section of a plasma-sprayed zirconia thermal barrier coating under corrosion test conditions.

Probably the most significant aspect of the plasma sprayed deposition method are the high cooling rates associated with the molten deposit hitting the substantially cooler substrate. Van Valzah and Eaton have recently completed work on the effect of cooling rates on the tetragonal → monoclinic transformation, thermal expansion behavior, and flexure strength of the plasma sprayed thermal barrier coatings [Ref. 27]. Their research indicates that t-ZrO_2 actually consists of two phases of ZrO_2. Metastable tetragonal (t') phase and another phase consisting of cubic and monoclinic ZrO_2. The metastable t' phase forms when the atomized ZrO_2 strikes the much cooler substrate and transforms rapidly from cubic to t'. The t' phase is termed 'non-transformable' due to a higher concentration of Y_2O_3 in t' than

tetragonal (t) phase. The t' phase undergoes phase separation via diffusion at temperatures greater than 1200°C [Ref. 27]. This phase separation will allow for a greater amount of tetragonal to monoclinic transformation upon cooling, leading to excessive microcracking and eventual coating failure.

The above findings occur for aged samples above 1200°C, the same principle can apply to lower temperature coatings. Although the plasma spray deposition method can lay down an even thin coating of material, the composition of the coating is harder to control. Phase segregation can occur during processing (laying a coating down). The dispersion of Y_2O_3 can not be controlled. The plasma spray method thus has some problem controlling precipitate size. Van Valzah and Eaton along with Lange also report that grain size of a critical diameter will also effect the t → m transformation [Ref. 25] and [Ref. 27]. Precipitate tetragonal grains larger than a d_c will transform spontaneously upon cooling. Tetragonal precipitates smaller than d_c but larger than a minimum diameter (d_m), are metastable at room temperature, but may transform in the front of a propagating crack. Grains smaller than d_m are stable at room temperature [Ref. 25] and [Ref. 27].

It is easy to understand that the method of fabrication can play an important role on the durability of thermal barrier coatings. Methods of application/fabrication which can produce a homogeneous spatial distribution would appear to have the ability to control the aforementioned problems of a phase segregation and control of critical grain size.

B. SURFACE INDUCED COATING METHOD

The fabrication/processing of ceramic composites can show improved mechanical properties with improved spatial distribution of toughening agents within the ceramic matrix. Recent studies by Jang and Moon on zirconia toughened alumina (ZTA), and Al_2O_3-ZrO_2-$SiC_{(w)}$ whisker composites utilizing colloidal science with interfacial electrochemistry has developed superior microstructures with uniform size and spatial distributions of both matrix and dispersed phases in these two systems [Ref. 24] and [Ref. 28].

The keys to the success of creating a ZTA composite powder by the surface induced coating (SIC) method are: (1) the determination of a pH range for a kinetically stable Al_2O_3 dispersion (a pH range where Al_2O_3 particles do not coagulate); (2) the determination of a pH range which will enhance the interfacial concentration of ionic species used for selective formation of the ZrO_2 precursor only at the interface (a pH range which enhances ZrO_2 formation on the Al_2O_3 particle); (3) the pH range which optimizes the first two conditions [Ref. 28]. The reader is encouraged to read reference 24, and reference 28 for a precise presentation and theoretical analysis of the SIC method. A flow diagram for the processing of Al_2O_3-ZrO_2-$SiC_{(w)}$ composite is shown in Figure 19 [Ref. 24].

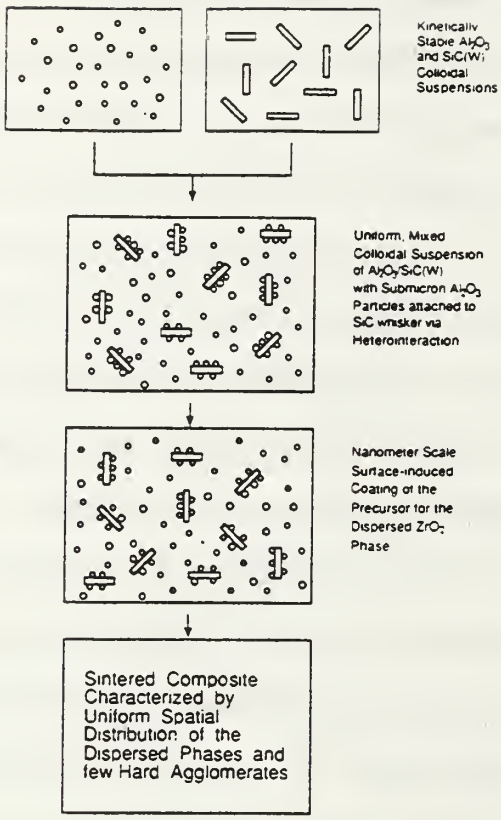

Figure 19. Schematic representation of homogeneous fabrication of Al_2O_3-ZrO_2-$SiC_{(W)}$ whisker composite by surface-induced coating.

Homogeneously coated ZTA powder samples (10 vol.% ZrO_2) were pressurelessly sintered at 1500°C for six hours. XRD analysis indicated that nearly 95 percent of the ZrO_2 grains remained tetragonal down to room temperature. Mechanically mixed samples were also prepared, sintered and cooled for comparison. Figure 20 shows outstanding results of scanning electron microscopy (SEM) photographs for both the SIC method (20(a)) and mechanically mixed microstructures (20(b)) [Ref.28].

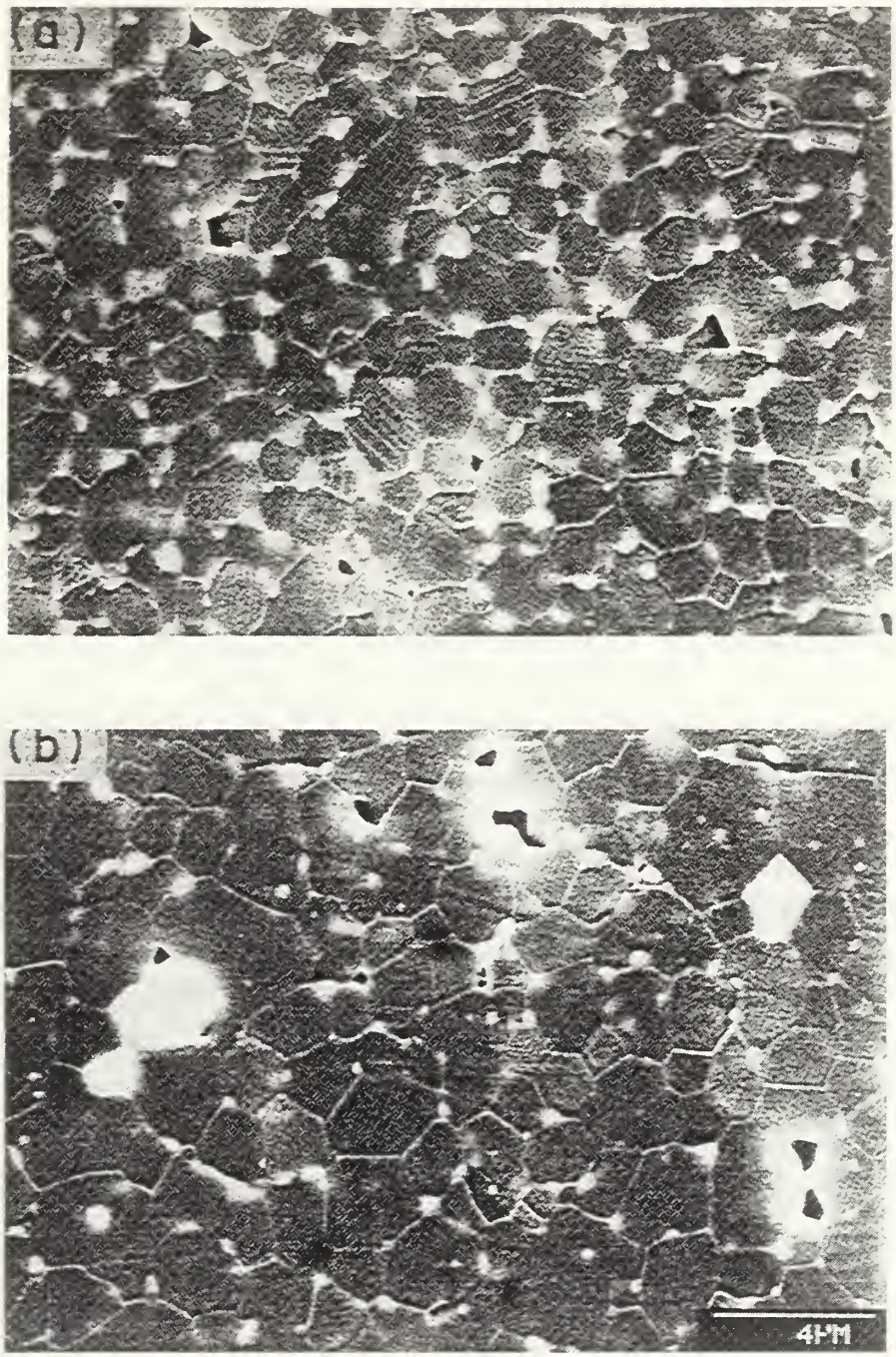

Figure 20. Scanning electron micrographs showing polished microstructures of zirconia-toughened alumina prepared by (a) surface-induced coating and (b) conventional mixing.

As shown by Figure 20(a), the microstructure is characterized by a uniform spatial distribution of the dispersed tetragonal ZrO_2 phase throughout the composite and by the absence of large ZrO_2 grains formed from hard ZrO_2 agglomerates. Figure 20(b) indicates that there are large cracklike voids produced by large hard ZrO_2 agglomerates, and is the main fracture origin for ZTA composites. These voids tend to propagate to a ZrO_2 deficient region [Ref. 28].

Returning to the idea of critical grain sizes, the surface induced coating sample intergranular ZrO_2 grain sizes were predominately under 1 μm (micro meter) in diameter, indicating that the martensitic t → m transformation was suppressed [Ref. 24]. Whereas the mechanically mixed sample had a wider range of grain sizes, making the sample much more susceptible to unfavorable t → m transformation. Figure 21 shows a comparison of matrix and dispersed phase grain sizes for both prepared samples [Ref. 24]. Ultrafine ZrO_2 grains (~ 0.1 μm or less) are unable to give transformation toughening due to the transformation resistance to monoclinic symmetry [Ref. 28].

The creation of a uniform spatial distribution of dispersed phase within the matrix phase is the result of the uniform coating of the ZrO_2 particles on Al_2O_3 particles, effectively pinning the Al_2O_3 grain boundaries and limiting the abnormal growth of Al_2O_3 grains.

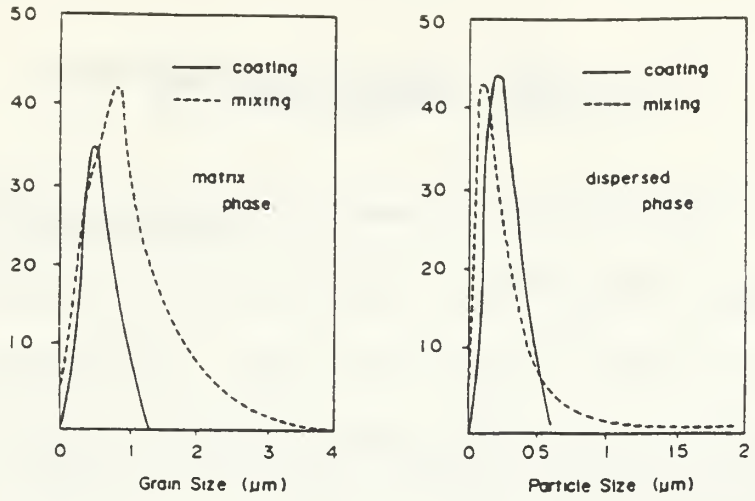

Figure 21. Grain size distribution of Al_2O_3 (matrix phase) and ZrO_2 (dispersed phase) in ZTA samples processed by two different methods, surface-induced coating and conventional mixing.

The addition of $SiC_{(w)}$ also provides additional strengthening mechanisms to the matrix by crack deflection, crack bridging, and whisker pullout. The control of the t → m transformation can enhance mechanical properties via the process zone mechanism [Ref. 24]. When the t → m transformation is not uniform and excessive, degradation of the thermal barrier coating will be accelerated. The Al_2O_3-ZrO_2-$SiC_{(w)}$ composite shows a three to four fold increase in rupture strength and fracture toughness, and just as important, the ability to control the microstructure of the ceramic matrix and avoid the degrading behavior of excessive t → m transformation. [Ref. 8] For these reasons, it is emphasized that the surface induced coating method be investigated as a possible alternative for the processing of yttria stabilized zirconia.

IV. SCOPE OF PRESENT WORK

Based upon previous research and literature introduced here, a summary of important conclusions is presented:

- ZrO_2 reacts slowly to form ZrV_2O_7 from Lewis-acid base theory.
- Y_2O_3 reacts on an equimolar basis with V_2O_5 to form YVO_4 very quickly which destabilizes the zirconia matrix, thereby increasing the chances of the t → m transformation.
- Application/fabrication processes for CMCs can directly impact the mechanical characteristics of ceramic composites.
- Addition of strengthening agents such as corundum and $SiC_{(w)}$ have been shown to improve both fracture toughness and strength values of CMCs.

The present work will involve mixing alpha alumina in varying concentrations to $ZrO_2$8mol%Y_2O_3 and exposing these samples to vanadium pentoxide for 100 hours at 900°C. Analysis by X-Ray Diffraction (XRD) and Scanning Electron Microscopy (SEM) will be used to:

- Re-investigate the reaction between V_2O_5 and $ZrO_2$8mol%Y_2O_3 in air at 900°C to verify the destabilization of tetragonal zirconia to the monoclinic polymorph.
- Determination of the degree of reactivity of α-Al_2O_3 in the pseudo ternary $ZrO_2$8mol%Y_2O_3-Al_2O_3-V_2O_5 system.

V. EXPERIMENTAL PROCEDURE

A. SAMPLE PREPARATION

Fine powder of yttria stabilized zirconia (TOSOH-Zirconia TZ-8Y $ZrO_2$8mol%Y_2O_3) were provided by TOSOH Corp., Tokyo, Japan. Vanadium pentoxide (V_2O_5 - 99.6% pure, Chlorine 0.15%, and Carbon Dioxide 0.09%), was provided by J.T. Baker Chemical Co., Phillipsburg, N.J., and alpha alumina (1.0 micron diameter), provided by BUEHLER LTD., Evanston, Illinois.

An accurate balance (Sartorius-Werke AG), was used in preparing ten 5.00 gram samples of varying concentrations of PSZ, V_2O_5, and Al_2O_3. Samples are presented in weight percent form in TABLE II. Each sample was mechanically mixed and placed in a Platinum (Pt) crucible and annealed at 900$\pm$15°C for 100 hours.

B. X-RAY DIFFRACTION

Each sample prior to annealing (mechanically mixed state), was run through the XRD to obtain a baseline value for comparison with a post-fired sample. In both samples, the powder sample was passed through a U.S. Standard #400 sieve mesh (38μm) and then mounted into a standard specimen holder and held in place by applying drops of acetone to 'cement' the sample in place. Excess powder and acetone residue was

removed by packing and smoothing with a razor blade to obtain a flat smooth surface.

X-Ray Diffraction was performed utilizing a Phillips XRG 3100 X-Ray generator, a PW 1710 Diffractometer controller, and directed by a Digital 3100 VAX work station. The X-Ray generator utilizes a copper target (Cu alpha 1,2 wavelengths = 1.54060, 1.54439 A respectively), with power settings of 30 kV and 35 mA. The gonio scan program was set with a 2θ angle range of 10-140 degrees, step size of 0.05 degrees, and scan rate of 10.0 seconds (for a total run time of 7:13:20). This scanning program and power setting was suitable for collecting all the raw data necessary for analysis.

Raw data files for each sample (pre and post annealed samples) were analyzed by using the VAX work station and the Phillips APD1700 software package. Peak positions and integrated intensities were calculated and recorded with each peak curve fitted for each sample. A matching program provides a probability that the constructed intensity curves 'match' other known intensity profiles on file within the software database. The match and analysis program was too vague in many instances and did not correlate well with small percentage (by weight percent) compounds that were expected in the analyzed sample. The Phillips PW 1891 Total Access Diffraction Database (TADD), PDF-2 sets 1-41, was

indispensable in using the 'search and match' method necessary in determining compounds within the powder sample.

C. SCANNING ELECTRON MICROSCOPY (SEM)

There was one reacted sample that formed an extremely hard and brittle mass in the Pt crucible. With this sample it was not possible to obtain enough of the sample to conduct a proper XRD analysis (post annealed gonio scan). After successive attempts to clean the Pt crucible with concentrated HCL, enough of a sample was obtained from the bottom of the crucible to conduct an SEM analysis. The sample remnants were cold mounted, sanded and polished, and carbon coated to enhance conductivity.

The microstructure of the mounted sample was studied on a Cambridge Model S200 Scanning Electron Microscope utilizing a LaB_6 gun, and equipped with a Kevex x-ray energy dispersive spectrometer (EDX). Chemical analysis was also measured by EDX to confirm observations resulting from X-Ray Diffraction analysis. The SEM backscattered imaging method was used to improve detection of the phases present using atomic number contrast.

TABLE II.

POWDER SAMPLES OF THE $ZrO_2$8mol.%Y_2O_3-Al_2O_3-V_2O_5 SYSTEM BY WEIGHT PERCENT

Sample No.	$ZrO_2$8mol.%Y_2O_3	Al_2O_3	V_2O_5
1	80	10	10
2	90	5	5
3	70	20	10
4	60	30	10
5	50	40	10
6	10	80	10
7	20	70	10
8	30	30	40
9	40	40	20
10	10	10	80

VI. RESULTS AND DISCUSSION

A. X-RAY DIFFRACTION RESULTS

1. YSZ-Al_2O_3-V_2O_5 Unreacted Powder Samples

All ten samples were analyzed by XRD analysis prior to annealing at 900°C for 100 hours. Samples analyzed indicated that all expected peak intensity and line positions accurately reflected the Hanawalt JCDP diffraction patterns verifying the phases present. Figure 22 shows sample number four plotted against each compound's diffraction pattern expected in the sample. Each compound's maximum intensity line is marked on the appropriate raw data peak. SCHERBINAITE (V_2O_5) has a peak intensity at the (001) reflecting plane, CORUNDUM (α-Al_2O_3) peak intensity at (113), and tetragonal ZrO_2 at (101).

2. YSZ-Al_2O_3-V_2O_5 Annealed Powder Samples

Assuming that the reaction between V_2O_5 and Y_2O_3 occurs on an equimolar basis, as shown by equation (2), and that ZrV_2O_7 forms after long periods of time, the expected phases present in the reacted samples can be calculated by converting the weight percentage of mixed constituents and converting them to atomic percent. Calculation of atomic percent is conducted by dividing each compound's gram weight percentage by the molecular formula for that compound. The atomic weights are then added to obtain the total molecular weight for each

sample. Atomic percentages can then be obtained by dividing each compound's atomic weight by the total molecular weight for that sample. TABLE III presents the expected atomic percentages for phases present in each reacted sample.

a. *Destabilization of ZrO_2*

Determination of ZrO_2 destabilization is rather straightforward with a formula which is simply the ratio of monoclinic peak intensity (111) plane, over the summation of monoclinic plus tetragonal peak intensity (101) plane [Ref. 23]:

$$\% \text{ Destabilization} = M/[M + T] \times 100$$

Figure 23 shows a comparison of a reacted and un-reacted sample (sample number one - 80%YSZ-10%Al_2O_3-10%V_2O_5), with marked peak heights for the tetragonal and monoclinic phases, along with the diffraction patterns for tetragonal ZrO_2, BADDELEYITE (monoclinic ZrO_2), and cubic ZrO_2.

An expanded view of Figure 23 is shown in Figure 24. Analysis of all other samples with ten percent V_2O_5, (samples one, three, four, five, six, and seven) indicates that the average destabilization from tetragonal to monoclinic ZrO_2 is nearly 95 percent complete.

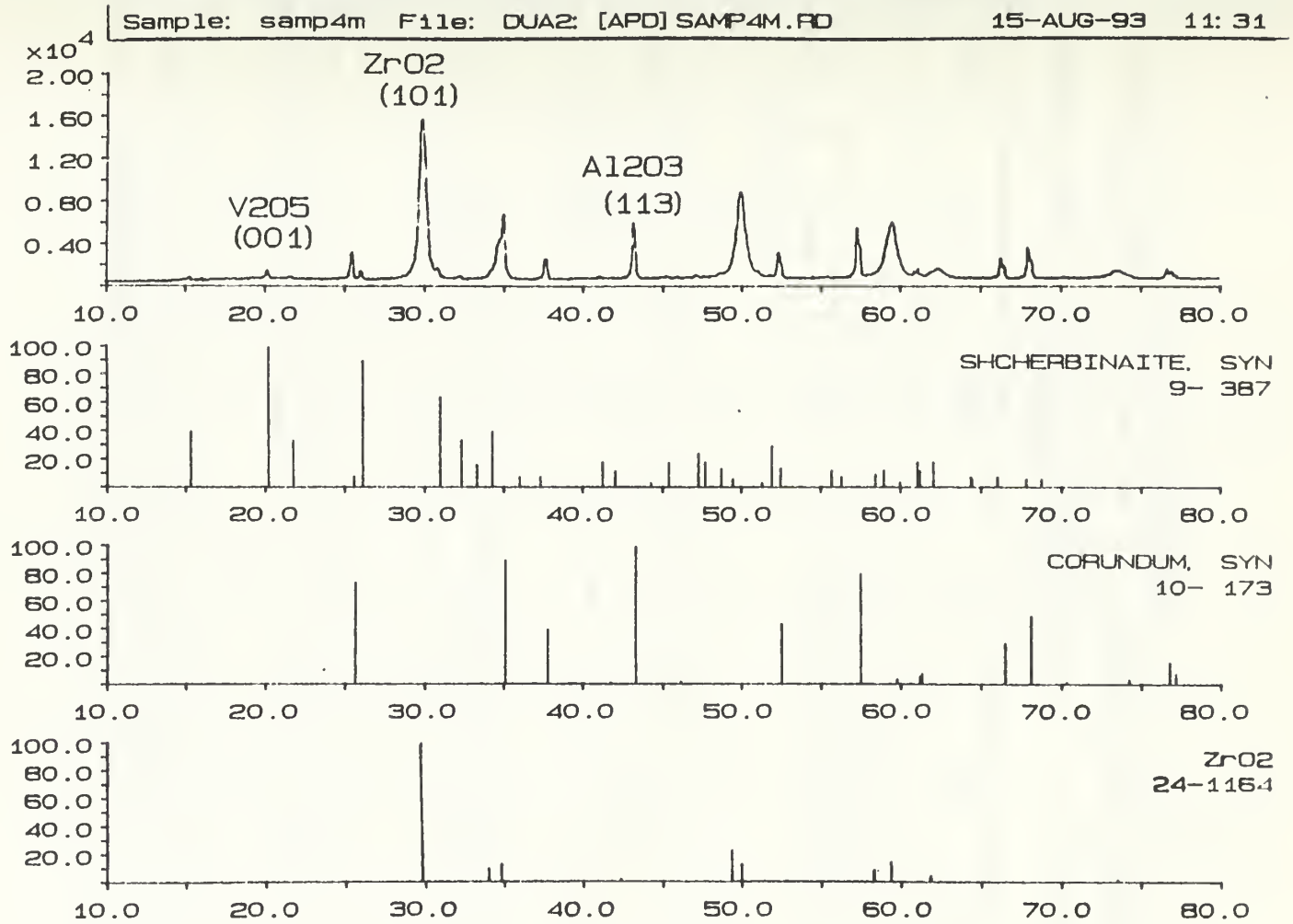

Figure 22. Plot of sample No.Four (60%YSZ-30%Al_2O_3-10%V_2O_5) and corresponding diffraction patterns for SCHERBINAITE, CORUNDUM, and tetragonal ZrO_2.

TABLE III.

ANNEALED POWDER SAMPLES OF THE $ZrO_2$8mol.%Y_2O_3-Al_2O_3-V_2O_5 SYSTEM

BY ATOMIC PERCENT

Sample #	ZrO_2	Al_2O_3	YVO_4	V_2O_5	Y_2O_3
1	73.15	12.87	12.78	0.82	-----
2	82.75	6.49	7.22	-----	3.58
3	62.51	25.43	10.87	1.58	-----
4	52.12	36.51	9.06	2.29	-----
5	42.28	47.39	7.35	2.96	-----
6	7.64	85.68	1.32	5.34	-----
7	15.66	76.81	2.72	4.79	-----
8	28.28	39.62	4.91	27.16	-----
9	34.71	48.63	6.03	10.61	-----
10	11.39	15.97	1.98	70.64	-----

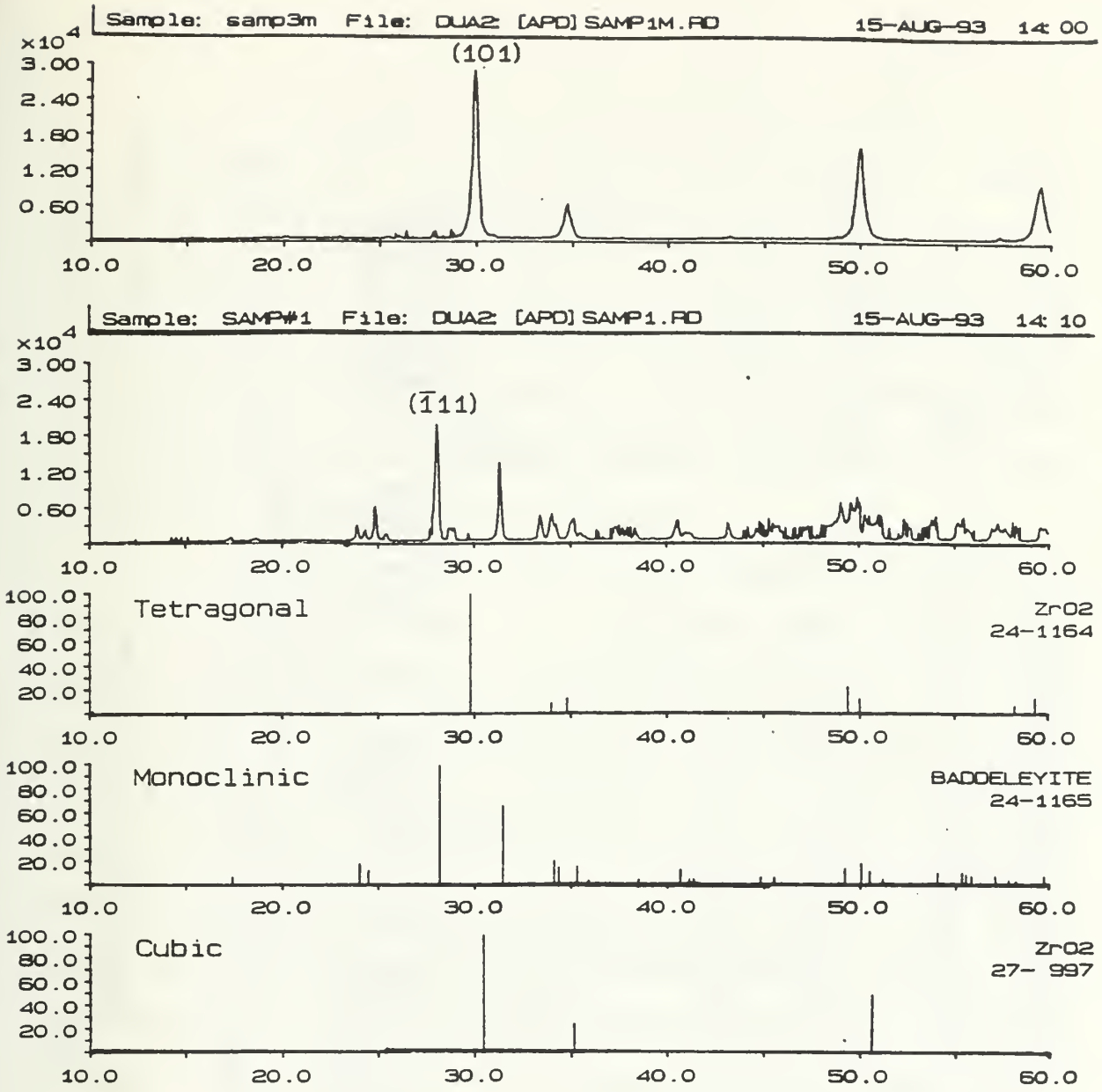

Figure 23. Comparison of sample number one (80%YSZ-10%Al_2O_3-10%V_2O_5) unreacted and reacted samples showing the three polymorph diffraction patterns for ZrO_2.

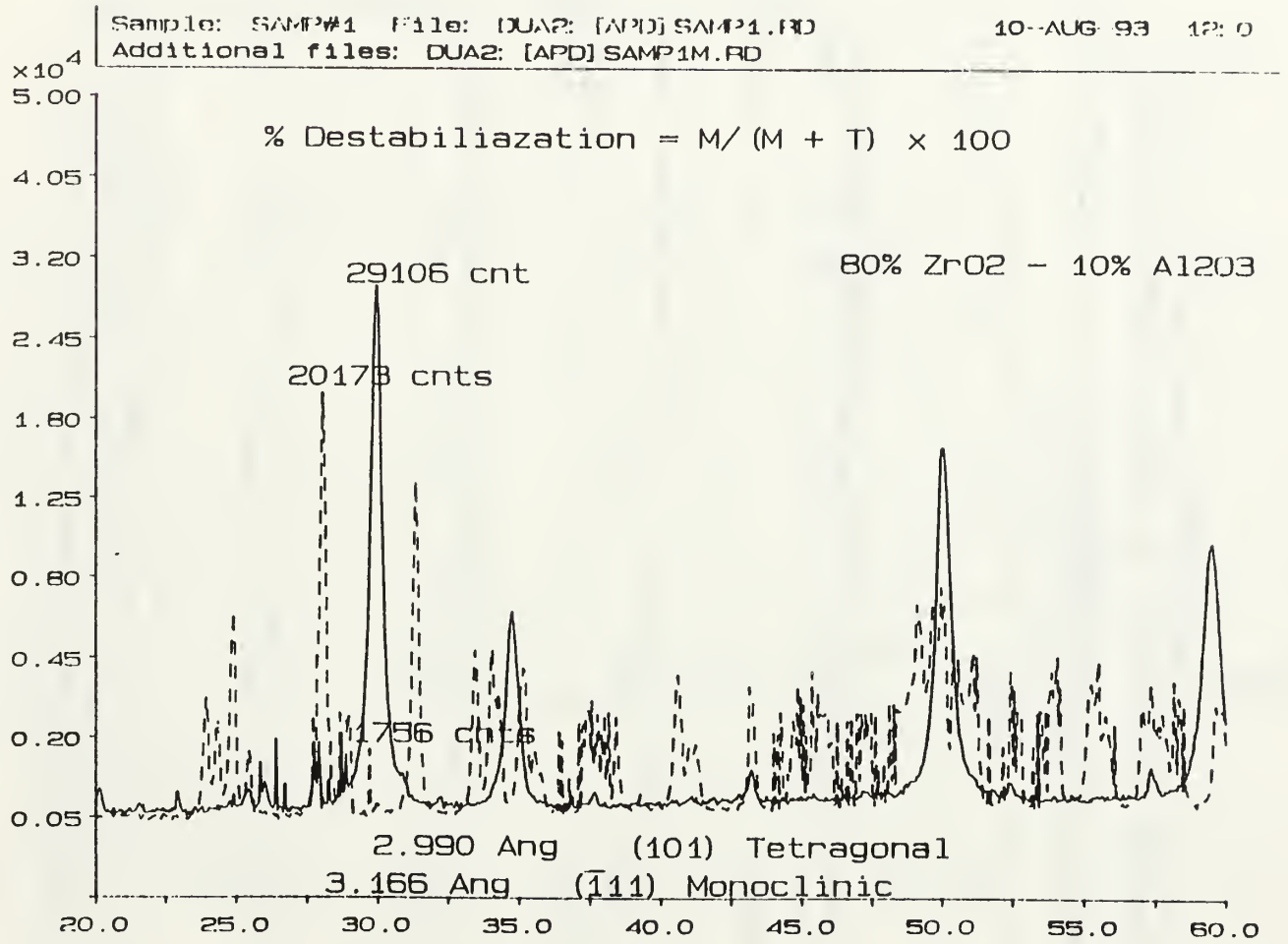

Figure 24. Measurement for percent destabilization for sample No. One.

Peak intensity values for monoclinic ZrO_2 from all reacted samples are listed in TABLE IV by increasing atomic percent ZrO_2. A plot of peak intensity versus atomic percent ZrO_2 is shown in Figure 25. Of significant interest in Figure 25 is the sharp increase in intensity at 28.3 atomic percent, and sharp decrease in intensity at 82.7 atomic percent ZrO_2. One possibility for the major jump in intensity is the formation of an amorphous glassy phase.

Sample number eight had an abundance of V_2O_5 by weight and atomic percent. It is possible that with a glass phase formation that some phases were "hidden" from XRD analysis and were under-counted, while other phases were over-counted giving the impression that more percent phase is actually present. The second peculiarity on this graph is from sample number two (82.7 atomic percent ZrO_2). This vast drop can be explained by equation (2), and viewing the expected results as shown in TABLE III. The results show that there is a significant drop in monoclinic ZrO_2, however it is noteworthy to say that sample number two is the only sample that calculates excess Y_2O_3, thereby indicating that all the V_2O_5 that could be consumed was used. A plot of reacted and un-reacted sample number Two raw data files are shown in Figure 26, emphasizing that the monoclinic and tetragonal peaks co-exist after 100 hours at 900°C.

TABLE IV.

PEAK INTENSITY VALUES FOR (111) MONOCLINIC ZrO_2 BY INCREASING ATOMIC PERCENT ZrO_2

Sample Number	Atomic Percent ZrO_2	Peak Intensity for (111) ZrO_2
6	7.64	894
10	11.39	894
7	15.64	1,574
8	28.28	10,427
9	34.71	3,302
5	42.28	7,156
4	52.12	9,941
3	62.51	11,378
1	73.15	20,173
2	82.75	7,721

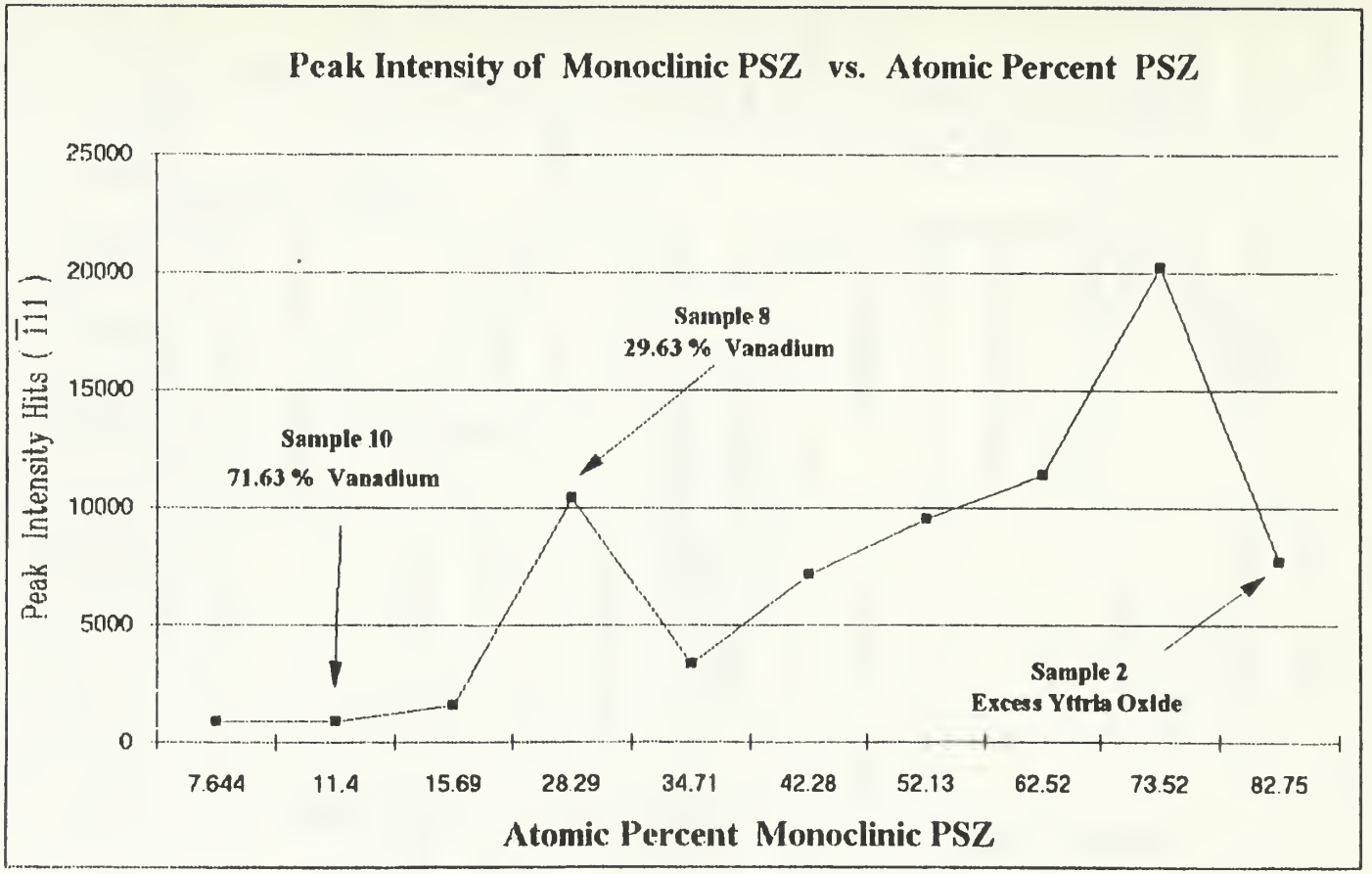

Figure 25. Peak intensity for monoclinic ZrO_2 ($\bar{1}11$) versus atomic percent monoclinic ZrO_2.

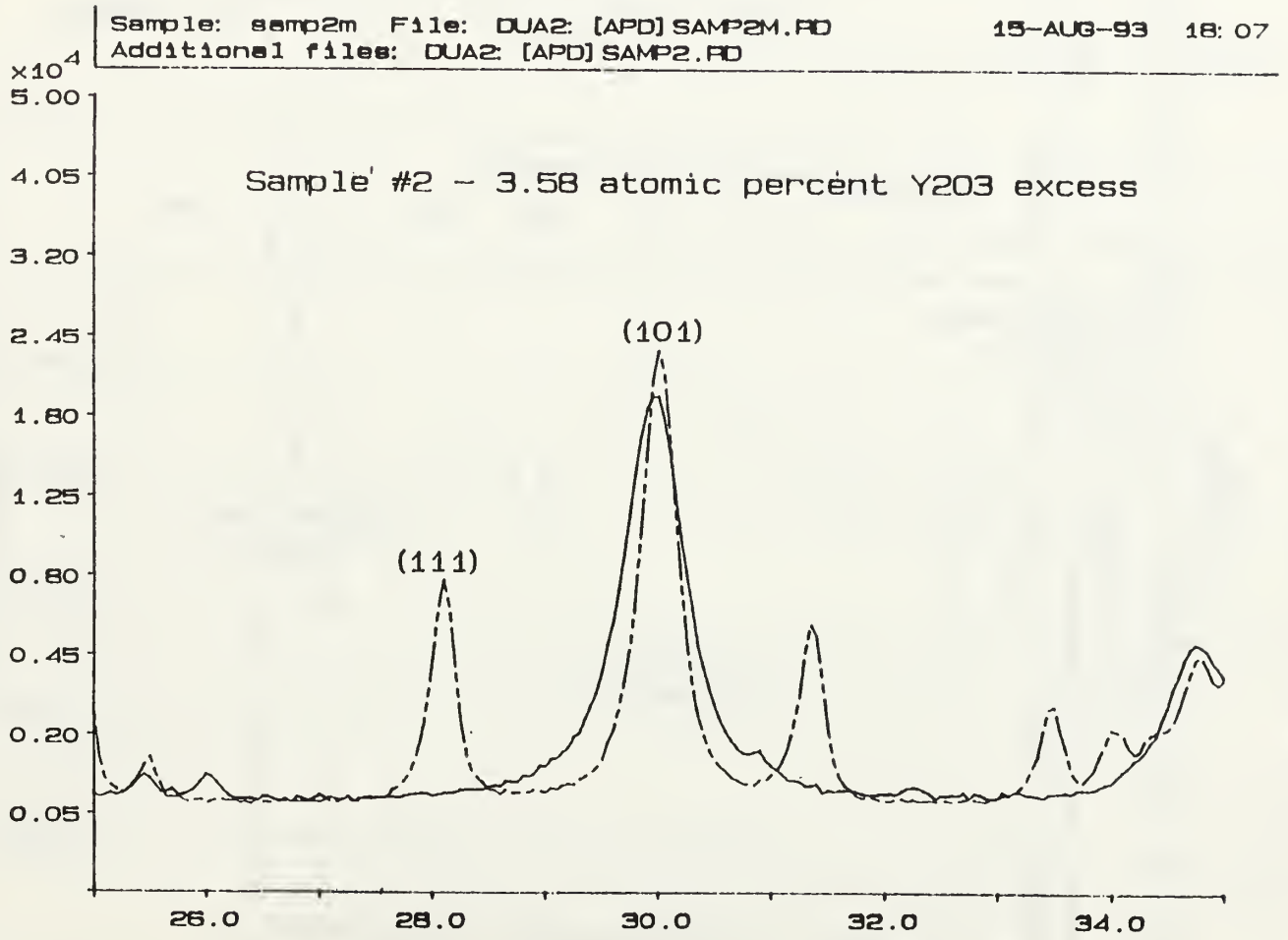

Figure 26. Plot of un-reacted and reacted sample No. Two showing both monoclinic and tetragonal ZrO_2 peaks.

b. Ytria Vanadate (YVO_4) Formation

As expected YVO_4 formation appears to occur rapidly and correlates well with the destabilization of ZrO_2. Figure 27 shows the tetragonal peak for YVO_4 at the (200) reflecting plane formed in sample number one. TABLE V presents the peak intensities for all samples by increasing atomic percent YVO_4. A plot of peak intensity versus atomic percent YVO_4 is displayed in Figure 28.

c. V_2O_5 Intensity

Vanadium pentoxide intensity readings support the YVO_4 formation reaction. The values obtained are somewhat sketchy in that two competing factors that impact the V_2O_5 intensity are at work. YVO_4 formation will deplete the amount of V_2O_5 available for diffraction. On the other hand, the remaining V_2O_5 will become more dense and sharpen the intensity peaks observed by the XRD. This analysis is more complicated than the formation transformation from tetragonal to monoclinic ZrO_2. An example (sample number eight) of the V_2O_5 peak intensity plane (001) is shown in Figure 29.

d. α-Al_2O_3 Intensity

Peak intensity calculations for alpha alumina were conducted on all reacted and un-reacted samples at the (113) reflecting plane as shown in Figure 30. Peak intensity values for the (113) reflecting plane are displayed in TABLE VI by increasing atomic percent α-Al_2O_3. A plot of peak intensity

for the un-reacted and reacted samples versus atomic percent α-Al_2O_3 is presented in Figure 31 and presents some interesting results.

In all samples with the exception of two, samples numbers eight and ten intensity values increased after 100 hours of annealing at 900°C. The significance of sample number eight (40%V_2O_5 by weight) and sample number ten (80%V_2O_5 by weight) reporting sharply reduced intensity values corresponds well with the excessive monoclinic ZrO_2 peaks seen in Figure 25, and one of the excessive peaks of tetragonal YVO_4 seen in Figure 27. The logical conclusion would be the formation of an amorphous glassy phase in both of these samples, α-Al_2O_3 being less dense and being hidden by the glassy phase was under-recorded by the XRD.

The three plots (α-Al_2O_3, ZrO_2, and YVO_4) all share one thing in common and that is, the general shape of the plot with increasing atomic percent. The quasi-linear, exponential growth curve arises from the densification due to annealing (sharpening of the beam broadening), and increase in the mass absorption coefficient for the calculated relative intensity due to increasing atomic weight percent. [Ref. 29]

With the exception of samples number eight and ten, by relative measure it appears that α-Al_2O_3 does not react nor interfere with the $ZrO_2$8mol.%Y_2O_3-V_2O_5 system and corresponding reactions.

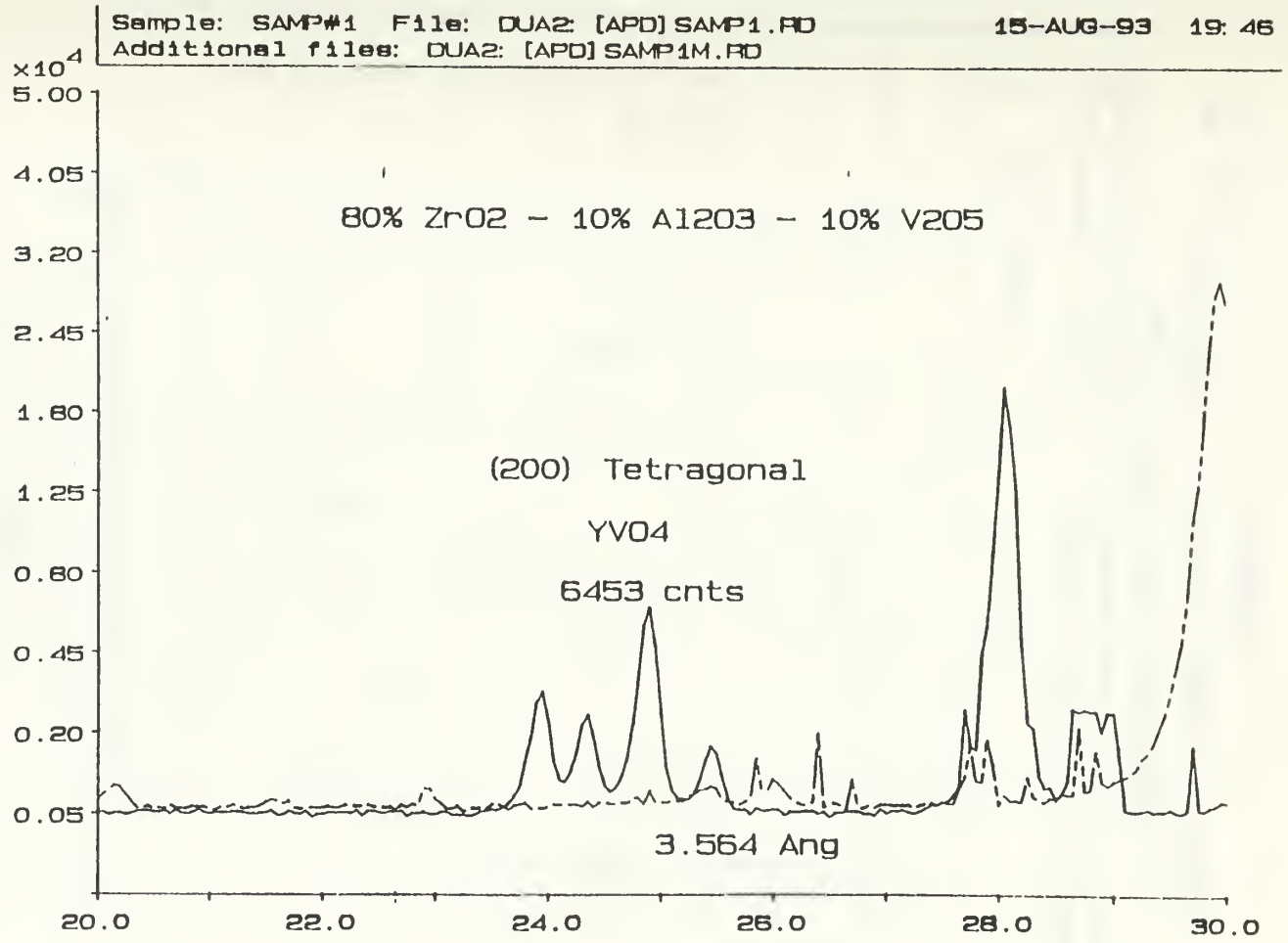

Figure 27. Plot of un-reacted and reacted sample No.One showing YVO_4 formation and peak intensity line for YVO_4 at the (200) reflection plane.

TABLE V.

PEAK INTENSITY VALUES FOR (200) TETRAGONAL YVO_4 BY INCREASING ATOMIC PERCENT YVO_4

Sample Number	Atomic Percent YVO_4	Peak Intensity (200) YVO_4
6	1.32	850
10	1.98	850
7	2.72	1,081
8	4.91	3,332
9	6.03	1,346
2	7.22	3,786
5	7.35	2,727
4	9.06	4,171
3	10.87	4,456
1	12.78	6,334

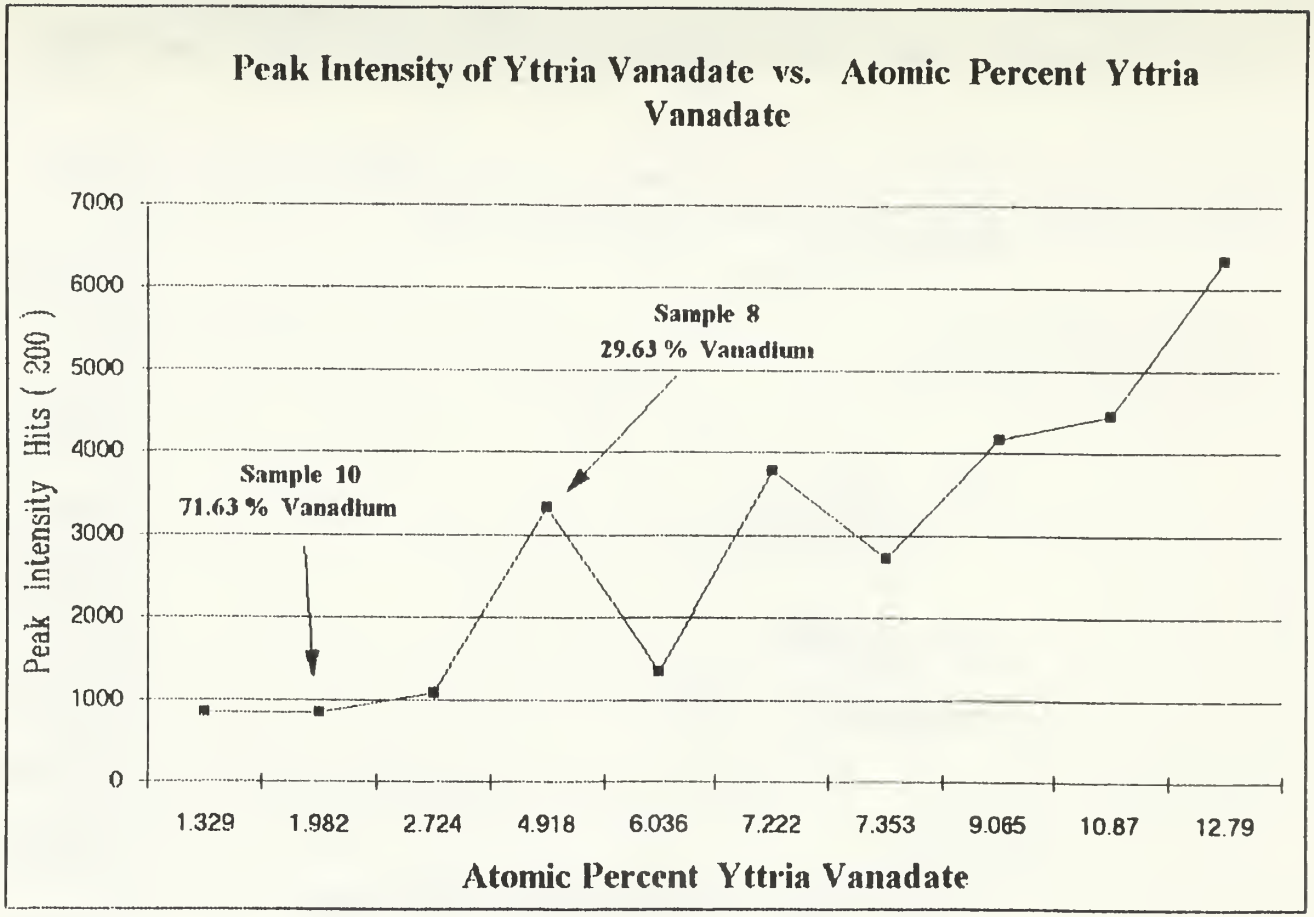

Figure 28. Plot of peak intensity of YVO_4 versus atomic percent YVO_4.

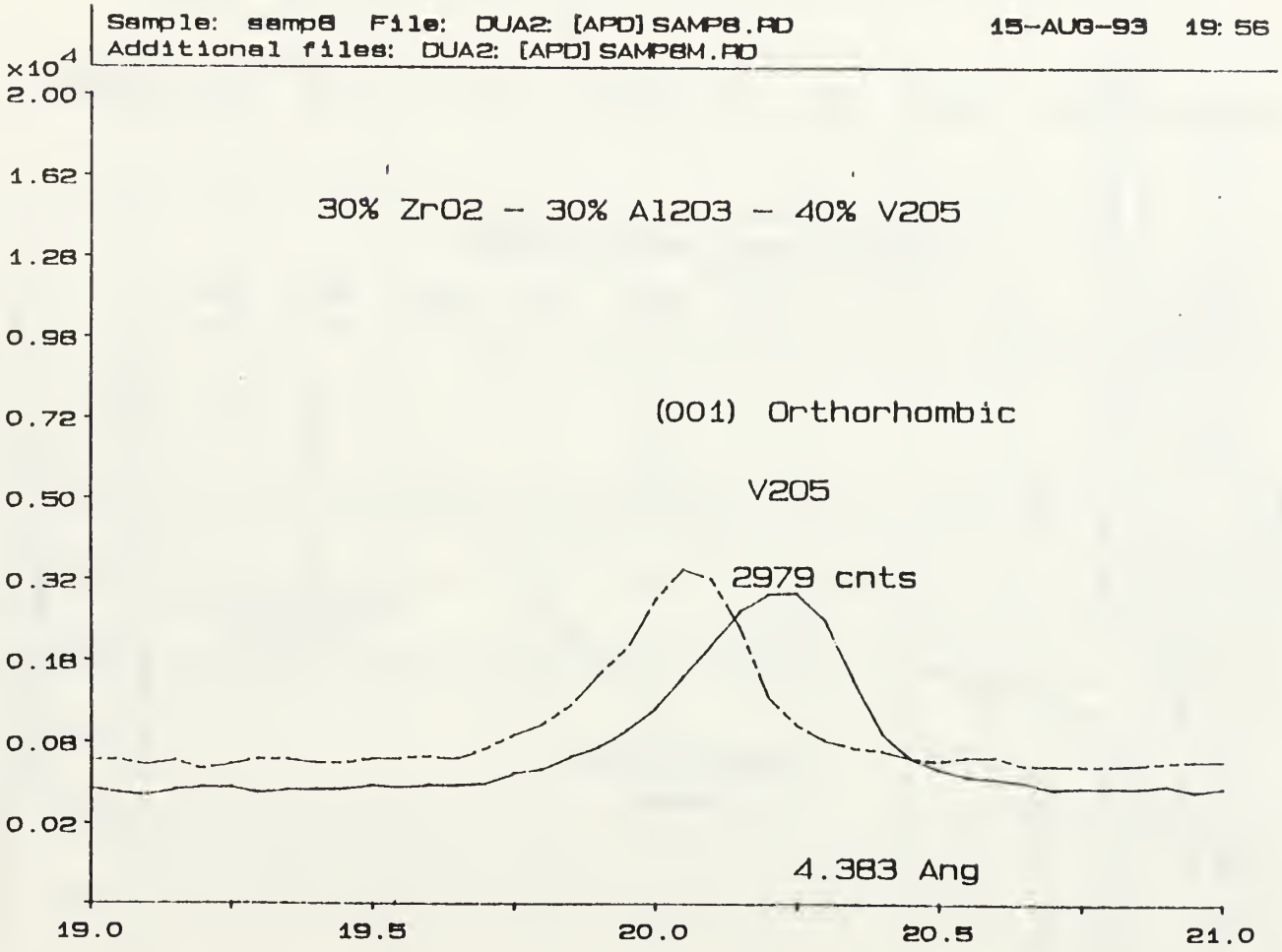

Figure 29. Plot of sample No. Eight V_2O_5 peak intensity (001) reflecting plane.

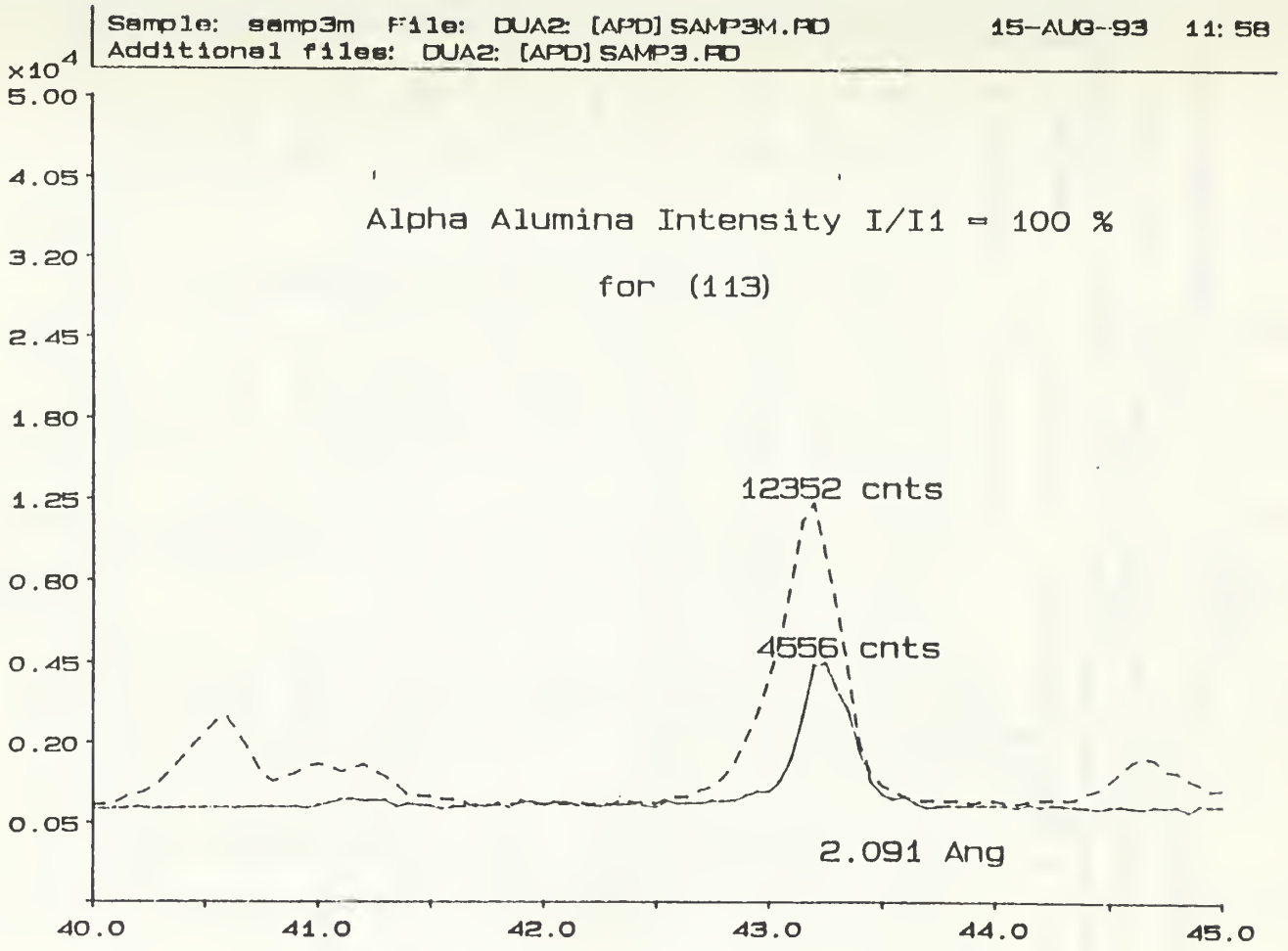

Figure 30. Comparison of un-reacted and reacted sample No.Three peak intensity values for (113) α-Al_2O_3 reflecting plane.

TABLE VI.

PEAK INTENSITY VALUES FOR (113) α-Al_2O_3 UNREACTED AND REACTED SAMPLES BY INCREASING ATOMIC PERCENT α-Al_2O_3

Sample Number	Atomic Percent α-Al_2O_3	Unreacted Intensity	Reacted Intensity
2	6.49	1,819	2,445
1	12.87	1,346	3,595
10	15.97	1,346	605
3	25.43	4,556	12,352
4	36.51	5,920	14,617
8	39.62	5,074	3,248
5	47.39	7,316	19,412
9	48.63	7,236	14,690
7	76.81	18,695	28,599
6	85.68	19,543	22,819

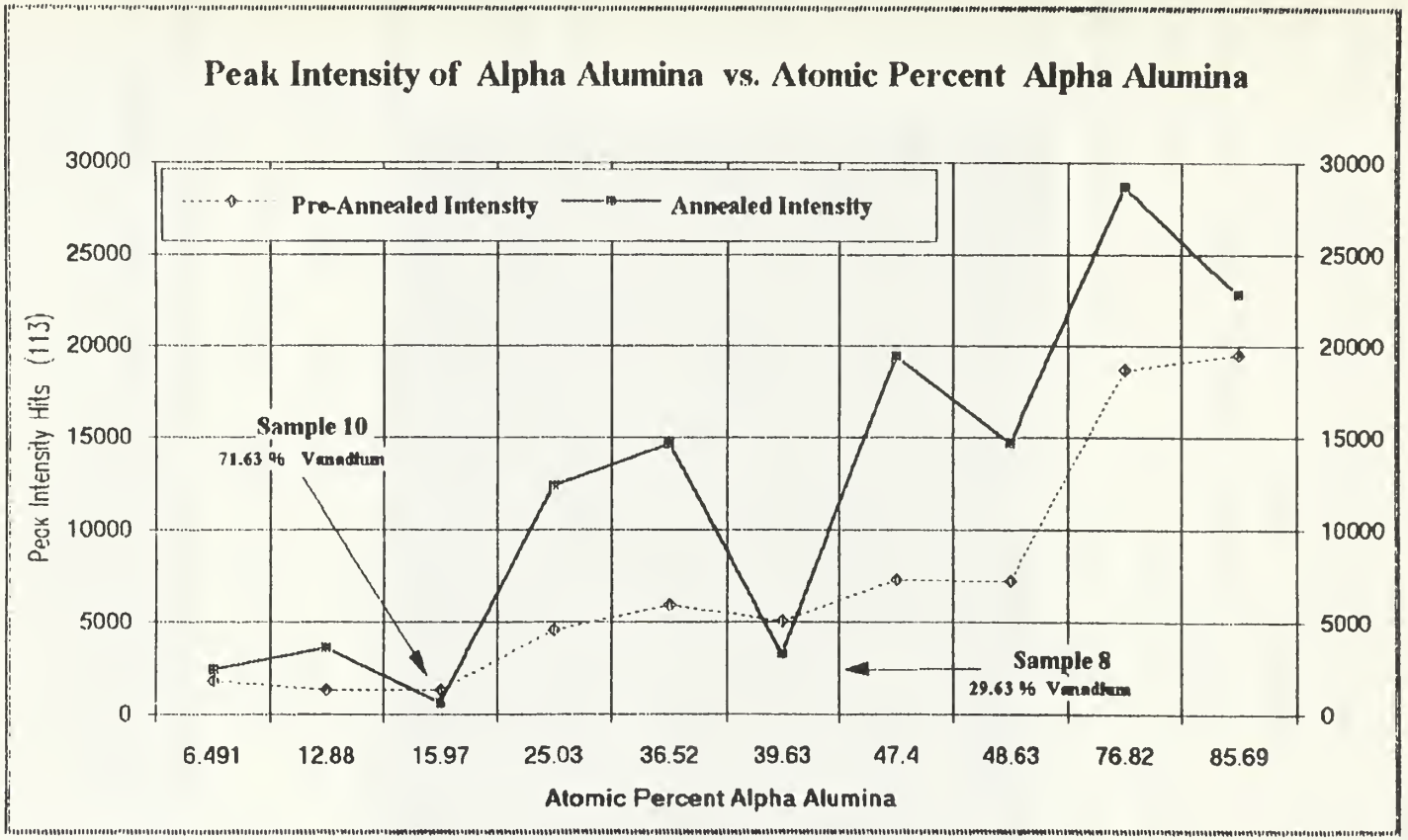

Figure 31. Plot of peak intensity (113) α-Al_2O_3 for un-reacted and reacted samples versus atomic percent α-Al_2O_3.

B. SEM RESULTS

Two samples were cold mounted from sample number ten (10%ZrO_2-10%Al_2O_3-80%V_2O_5). Samples were obtained from the bottom of the Pt crucible after repeated saturation cleanings with concentrated HCl acid. Only one of the two specimens survived final polishing with a 1.0 micron diamond compound. SEM photographs and EDX analysis prove the formation of a glassy phase in samples number eight and ten, thereby substantiating previous explanations for variations in intensity for the ZrO_2, YVO_4, and α-Al_2O_3 plots. Figure numbers 32, 33, and 34 show a sequence of pictures taken of the same region and the chemical analysis by EDX for each respective view.

All three pictures show varying concentrations of oxides based upon location of the EDX probe. Figure 32 indicates the presence of all expected reactants with the exception of YVO_4. In fact, YVO_4 does not appear in any of these three pictures. Figure 33 is nearly 100 percent ZrO_2 (view of ZrO_2 agglomerate). Figure 34 taken to the left of the ZrO_2 agglomerate appears amorphous in nature and contains nearly 62 percent V_2O_5 (as compared to expected value by atomic percent calculation of 70.6 percent).

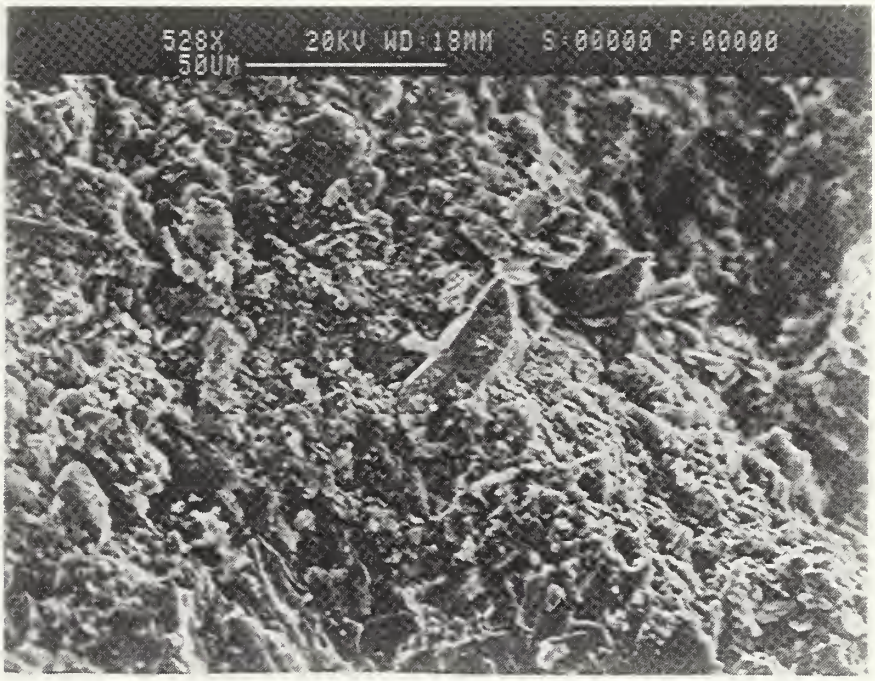

Figure 32. Wide field view of sample number ten (X528). EDX analysis by oxide percent: 22.75% ZrO_2, 15.35% Y_2O_3, 30.7% V_2O_5, and 31.83% Al_2O_3; Analysis by weight percent: 16.84% Al, 16.84%V, 12.09% Y, 16.84% Zr, and 37.83% O.

Figure 33. ZrO_2 agglomerate from sample number ten (close up view of Figure 32), (X1, 32K). EDX analysis by oxide percent: 95.17% ZrO_2, and 4.83% Y_2O_3; Analysis by weight percent: 3.8%Y, 70.46% Zr, and 25.74% O.

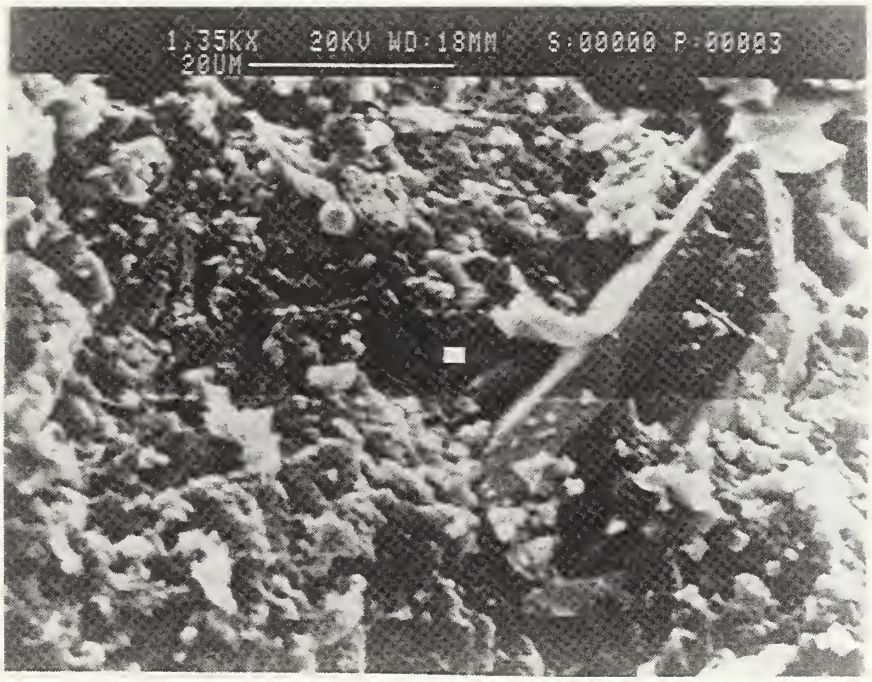

Figure 34. View of EDX probe on the matrix surface to the left of the ZrO_2 agglomerate (X1,35K). EDX analysis by oxide percent: 34.13% ZrO_2, 4.32% Y_2O_3, and 61.55% Al_2O_3; Analysis by weight percent: 34.48% V, 3.4% Y, 25.26% Zr, and 36.85% O.

Two very contrasting examples of the crystalline and amorphous nature of sample number ten are presented in Figures 35 and 36 respectively. In particular, Figure 36 shows a wave-like nature to the amorphous phase with the hint of α-Al_2O_3 just below and breaching the surface of the glass.

All of the SEM photographs taken for this sample clearly indicate partial glass formation due primarily to the high concentrations of V_2O_5 in this sample, explaining the behavior of peak intensity fluctuations versus atomic percent of compound in the ZrO_2, YVO_4, and α-Al_2O_3 plots (Figures 25, 28, and 31).

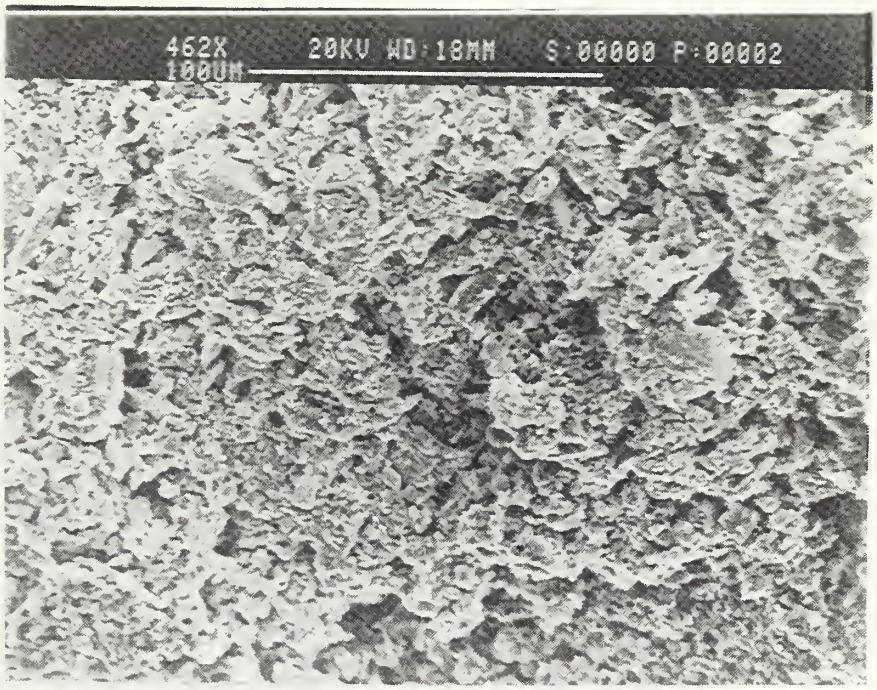

Figure 35. Broad view of crystalline structure for sample number ten (X462). EDX analysis by oxide percent: 24.93% ZrO_2, 7.06% Y_2O_3, 33.04% V_2O_5, and 34.97% Al_2O_3; Analysis by weight percent: 18.51% Al, 18.51% V, 5.56% Y, 18.46% Zr, and 38.97% O.

Figure 36. Amorphous glassy phase of sample number ten (X236). EDX analysis by oxide percent: 26.88% ZrO_2, 35.52% V_2O_5, and 37.6% Al_2O_3; Analysis by weight percent: 19.9% Al, 19.9% V, 19.9% Zr, and 40.3%O.

VII. CONCLUSIONS

Investigation of the pseudo-ternary $ZrO_2$8mol.%Y_2O_3-Al_2O_3-V_2O_5 system using X-ray diffraction and SEM analysis indicates the following:

- The exposure of powder samples to V_2O_5 at 900°C for 100 hours was sufficient to destabilize the Yttria stabilized zirconia.
- YVO_4 formation occurs rapidly and corresponds in relative intensity measurement to the increase in monoclinic ZrO_2.
- In all the samples analyzed there was no supportive evidence for the formation of zirconium divanadate (ZrV_2O_7).
- Comparison of α-Al_2O_3 peak intensities at the (113) reflecting plane for unreacted and reacted powder samples indicates that α-Al_2O_3 is non-reactive with the $ZrO_2$8mol.%Y_2O_3-V_2O_5 compounds. Samples eight and ten showed decreased (113) intensity values due to the formation of an amorphous glassy phase.

VIII. RECOMMENDATIONS

With the appearance that α-Al_2O_3 is non-reactive with the $ZrO_2$8mol.%Y_2O_3-V_2O_5 system , the next logical step is to test the strength and fracture toughness values of this composite by fabricating test coupons and subjecting them to operational type conditions, i.e., corrosive environment and thermal cycling to and from operating temperatures.

To address the desire of increased service life from corrosive destabilization, the fabrication process should be one which can best produce a homogeneous microstructure with spatially distributed reinforcements. The surface induced coating method should be thoroughly investigated as this process holds the promise of minimizing the destabilization of tetragonal to monoclinic ZrO_2 from YVO_4 formation.

During the literature review it was apparent that researchers are currently looking at alternative stabilizers to replace yttria oxide. Based on Lewis acid-base theory other stabilizers (which are more acidic than Y_2O_3) like Sc_2O_3 and I_2O_3 have shown promising results in the reduction of VO_4 formation. Again however, even the use of these stabilizers should be looked at with the idea of utilizing a fabrication

process which could produce the much desired homogeneous microstructure.

LIST OF REFERENCES

1. D. W. Susnitzky, W. Hertl, and C. B. Carter, Destabilization of Zirconia Thermal Barriers in the Presence of V_2O_5", *Journal of the American Ceramic Society*, Vol. 71, No. 11, pp. 992-1004, 1988.

2. E. Otero, A. Pardo, J. Hernandez, and F. J. Perez, "THE CORROSION OF SOME SUPERALLOYS (AT 1000K) IN MOLTEN EUTECTIC MIXTURE 60% V_2O_5-40% Na_2SO_4. THE INFLUENCE OF THE OXYGEN AND CARBON RESIDUES", *Corrosion Science*, Vol. 33, No. 11, pp. 1747-1757, 1992.

3. D. W. Susnitzky, W. Hertl, and C. B. Carter, "Vanadia-Induced Transformations in Yttria-Stabilized Zirconia", *Ultramicroscopy*, Vol. 30, pp. 233-241, 1989.

4. R. Ruh and T. J. Rockett, *Journal of the American Ceramic Society*, Vol. 53, No. 6, p. 360, 1970.

5. W. M. Kriven, W. L. Frasner, and S. W. Kennedy, in A. H. Heuer and L. W. Hobbs (eds.), *Science and Technology of Zirconia, Advances in Ceramics*, Vol. 3, pp. 82-97, American Ceramic Society, Columbus, Ohio, 1981.

6. E. C. Subbarao, A. H. Heuer and L. W. Hobbs (eds.), *Science and Technology of Zirconia, Advances in Ceramics*, Vol. 3, pp. 82-97, American Ceramic Society, Columbus, Ohio, 1981.

7. K. K. Chawla, **Composite Materials, Science and Engineering**, Springer-Verlag, New York, NY, 1987.

8. N. Claussen, "Strengthening Strategies for ZrO_2-toughened Ceramics at High Temperatures", *Materials Science and Engineering*, Vol. 71, pp. 23-28, 1985.

9. W. D. Tuohig and T. Y. Tien, *Journal of the American Ceramic Society*, Vol. 63, No. 9-10, pp. 595-596, 1980.

10. V. S. Stubican and J. R. Hellman, *Advancements in Ceramics*, Vol. 3, pp. 25-36, American Ceramic Society, Columbus, Ohio, 1981.

11. L. Lelait and S. Alperine, "T.E.M. Investigations Of High Toughness Non-Equilibrium Phases In The ZrO_2-Y_2O_3 System", *Scripta Metallurgica*, Vol. 25, pp. 1815-1820, 1991.

12. A. H. Heuer, R. Chaim, and V. Lanteri, "Review: Phase Transformations and Microstructural Characterization of Alloys in the System Y_2O_3-ZrO_2", *Advances in Ceramics,* Vol. 24, *Science and Technology of Zirconia III*, The American Ceramic Society, Inc., 1988.

13. V. Cirilli, A. Burdese, and C. Brisi, Atti Academy of Science Torino, Vol. 95, p. 14, 1961.

14. P. Doerner, L. J. Gauckler, H. Krieg, H. L. Lukas, G. Petzow, and J. Weiss, CALPHAD: Computer Coupling Phase Diagrams Thermochem., Vol. 3, No. 4, pp. 241-257, 1979.

15. T. Noguchi and M. Mizuno, *Kogyo Kogaku Zasshi*, Vol. 70, No. 6, pp. 839, 1967.

16. D. R. Askeland, **The Science and Engineering of Materials, 2nd Ed.**, PWS-KENT Publishing Co., Boston, Masachusetts, pp. 458-459, 1989.

17. L. A. Klinkova and E. A. Ukshe, *Zh. Nerg. Khim*, Vol. 20., No. 2, pp. 481, 1975; *Russian Journal of Inorganic Chemistry* (English Translation), Vol. 20, No. 2, p. 226, 1975.

18. E. M. Levin, *Journal of the American Ceramic Society*, Vol. 50, No. 7, p. 381, 1967.

19. R. L. Jones, "India as a Hot Corrosion-Resistant Stabilizer for Zirconia", *Journal of the American Ceramic Society*, Vol. 75, No. 7, pp. 1818-21, 1992.

20. C. F. Grain, *Journal of the American Ceramic Society*, Vol. 50, No. 6, p. 289, 1967.

21. F. M. Spiridonov, L. N. Popova, and R. Ya. Popilskii, *Journal of Solid State Chemistry*, Vol. 2, No. 3, p. 432, 1970.

22. R. L. Jones, "Oxide Acid-Base Reactions In Ceramic Corrosion", *High Temperature Science*, Vol. 27, pp. 369-380, 1990.

23. R. L. Jones, "The Development of Hot-Corrosion Resistant Zirconia Thermal Barrier Coatings", *Materials at High Temperatures*, Vol. 9, No. 4, 1991.

24. H. M. Jang, J. H. Moon, and C. W. Jang, "Homogeneous Fabrication of Al_2O_3-ZrO_2-SiC Whisker Composite by Surface-Induced Coating", *Journal of the American Ceramic Society*, Vol. 75, No. 12, pp. 3369-76, 1992.

25. F. F. Lange, "Transformation Toughening: Part 1, Size effects associated with the thermodynamics of constrained transformations", *Journal of Materials Science*, Vol. 17, pp. 225-234, 1982.

26. S. Chen and P. Shen, "Effect of NiO Dissolution on the Transformation of Plasma-sprayed Y-PSZ", *Materials Science and Engineering*, A 114, pp. 159-165, 1989.

27. J. R. VanValzah and H. E. Eaton, "Cooling rate effects on the tetragonal to monoclinic phase transformation in aged plasma-sprayed yttria partially stabilized zirconia", *Surface and Coatings Technology*, Vol. 46, pp. 289-300, 1991.

28. H. M. Jang and J. H. Moon, "Homogeneous fabrication and densification of zirconia toughened alumina (ZTA) composite by the surface-induced coating", *Journal of Materials Research*, Vol. 5, No. 3, pp. 615-622, 1990.

29. B. D. Cullity, **ELEMENTS OF X-RAY DIFFRACTION, 2nd Ed.**, ADDISON-WESLEY Publishing Co., Menlo Park, California, p. 18, 1978.

INITIAL DISTRIBUTION LIST

	No. Copies
1. Library, Code 52 Naval Postgraduate School Monterey, CA 93943-5002	2
2. Naval Engineering Curricular Office, Code 34 Naval Postgraduate School Monterey, CA 93943-5100	1
3. Prof. M. D. Kelleher, Code ME/Kk Chairman Department of Mechanical Engineering Naval Postgraduate School Monterey, CA 93943-5100	1
4. Prof. A. G. Fox, Code ME/Fx Department of Mechanical Engineering Naval Postgraduate School Monterey, CA 93943-5100	2
5. LT Dean M. Krestos 2058 Forest Gate Drive East Jacksonville, FL 32224	4
6. Mr. Joel S. Patton Code 2813 Annapolis Detachment of the Carderock Division Naval Surface Warfare Center Annapolis, MD 21402	1
7. Defense Technical Information Center Cameron Station Alexandria, VA 22304-6145	2

432.709

DUDLEY KNOX LIBRARY
NAVAL POSTGRADUATE SCHOOL
MONTEREY CA 93943-5101

GAYLORD S

AMERICAN BINDERY
6-94

DUDLEY KNOX LIBRARY
3 2768 00019150 6